Micron 151 (2021) 103160

Contents lists available at ScienceDirect

Micron

journal homepage: www.elsevier.com/locate/micron

Invited review

Finite-difference Time-domain (FDTD) Optical Simulations: A Primer for the Life Sciences and Bio-Inspired Engineering

Dakota E. McCoy [a,b,1], Anna V. Shneidman [c,*,1], Alexander L. Davis [d], Joanna Aizenberg [c,e]

[a] Department of Organismic and Evolutionary Biology, Harvard University, 26 Oxford Street, Cambridge, MA, 02138, USA
[b] Department of Materials Science and Engineering, Stanford University, Stanford, CA, 94305, USA
[c] John A. Paulson School of Engineering and Applied Sciences, Harvard University, 9 Oxford Street, Cambridge, MA, 02138, USA
[d] Department of Biology, Duke University, Campus Box 90338, Durham, NC, 27708, USA
[e] Department of Chemistry and Chemical Biology, Harvard University, 12 Oxford Street, Cambridge, MA, 02138, USA

ARTICLE INFO

Keywords:
Finite-difference time-domain
Optical simulation
Reflectance
Biological optics
Color science
Structural color

ABSTRACT

Light influences most ecosystems on earth, from sun-dappled forests to bioluminescent creatures in the ocean deep. Biologists have long studied nano- and micro-scale organismal adaptations to manipulate light using ever-more sophisticated microscopy, spectroscopy, and other analytical equipment. In combination with experimental tools, simulations of light interacting with objects can help researchers determine the impact of observed structures and explore how variations affect optical function. In particular, the finite-difference time-domain (FDTD) method is widely used throughout the nanophotonics community to efficiently simulate light interacting with a variety of materials and optical devices. More recently, FDTD has been used to characterize optical adaptations in nature, such as camouflage in fish and other organisms, colors in sexually-selected birds and spiders, and photosynthetic efficiency in plants. FDTD is also common in bioengineering, as the design of biologically-inspired engineered structures can be guided and optimized through FDTD simulations. Parameter sweeps are a particularly useful application of FDTD, which allows researchers to explore a range of variables and modifications in natural and synthetic systems (e.g., to investigate the optical effects of changing the sizes, shape, or refractive indices of a structure). Here, we review the use of FDTD simulations in biology and present a brief methods primer tailored for life scientists, with a focus on the commercially available software *Lumerical FDTD*. We give special attention to whether FDTD is the right tool to use, how experimental techniques are used to acquire and import the structures of interest, and how their optical properties such as refractive index and absorption are obtained. This primer is intended to help researchers understand FDTD, implement the method to model optical effects, and learn about the benefits and limitations of this tool. Altogether, FDTD is well-suited to (i) characterize optical adaptations and (ii) provide mechanistic explanations; by doing so, it helps (iii) make conclusions about evolutionary theory and (iv) inspire new technologies based on natural structures.

1. Introduction: What is FDTD and Why Is It Useful

Light is a fundamental force shaping the evolution of life on Earth. Many organisms use and manipulate light, from dinoflagellates photosynthesizing (Niyogi and Truong, 2013) to dinosaurs displaying iridescent feathers (Li et al., 2010). Photosynthetic and photoheterotrophic organisms depend on solar power and use physical and chemical processes to harvest energy from the sun (Holt et al., 2014; Jacobs et al., 2016). A plethora of sexually-selected animals use pigments and/or physical structures that interact with light to render themselves more attractive to potential mates (Hsiung et al., 2017; Wilts et al., 2014). Predators and prey camouflage their appearance, melting into shadows (Spinner et al., 2013; Stevens and Merilaita, 2011; Wilts et al., 2013), turning their bodies transparent (Johnsen, 2001; Bagge et al., 2017), and shining lights to lure (Haddock et al., 2005; Haygood and Distel, 1993) or befuddle (Esaias and Curl, 1972; Jones and Nishiguchi, 2004; Vacquié-Garcia et al., 2012; Widder, 1998; Young et al., 1980). Animals navigate their environment and interact with other organisms using eyes and other light-sensitive organs (Aizenberg et al., 2001; Palmer et al., 2017, 2018).

* Corresponding author.
E-mail address: ashneidm@g.harvard.edu (A.V. Shneidman).
[1] These authors contributed equally.

https://doi.org/10.1016/j.micron.2021.103160
Received 19 April 2021; Received in revised form 22 September 2021; Accepted 27 September 2021
Available online 1 October 2021

For decades, our understanding of light-dependent evolution has benefited from empirical measurements, dissections, and behavioral studies that unravel how and why organisms manipulate light. Little structures have big effects (Gorb, 2009): with the advent of sophisticated optical tools — high resolution optical microscopy, electron microscopy, and spectroscopy — biologists have been able to provide a detailed physical understanding of biological optics (Johnsen, 2012; Vukusic and Stavenga, 2009). Diverse biological structures can also inspire new sustainable technologies, such as bio-inspired solar power technologies (Siddique et al., 2017), sensors (Potyrailo et al., 2015; Sandt et al., 2018), and coatings (Hallam et al., 2009; Han et al., 2016; Xie et al., 2008). Often, microscopy reveals many structures whose functions can be hypothesized, but additional tools (e.g., spectroscopy or computer simulations) are necessary to identify exactly which portions are essential to the optical function, rather than serving another role such as mechanical support or fluid or thermal transport. In addition, theory or simulation can help reveal the relative contribution of each structure or phenomenon to the observed optical effect (discussed in more detail in Section 2.1). For example, does absorption or scattering dominate? What are the influences of variations in geometry and materials properties such as refractive index and absorption coefficient?

Optical simulation tools are a powerful complement to microscopy and theory to provide a holistic explanation of the observed optical effects. While analytical theory (writing and solving a set of equations by hand or on a computer) can be used to explain simple structures — such as the colors that arise from thin films of oil on asphalt — complex structures common in biology often require numerical simulation, in which numerical approximations to the physical equations are solved iteratively until they converge to a solution. Researchers can choose from many numerical simulation methods. For example, ray tracing simulations can be used in situations where objects are much larger than the wavelengths of light; finite element and finite difference methods are suitable when some or all dimensions of the object are comparable to the size of the wavelength of light (requiring more detailed physical treatment than larger objects); Monte Carlo simulations are often applied for random scattering media; and density functional theory and molecular dynamics model light absorption and other effects that depend on energy level structure or molecular-scale motion, respectively. Each method has its own advantages and disadvantages related to ease of use, relevance to the exact biological problem, and computational time. We provide a brief elaboration on the various methods in Section 3 and suggest that interested readers look to papers and textbooks on computational electromagnetics (e.g. Rylander et al., 2013; Sankaran, 2019; Sheng and Song, 2011).

In this tutorial, we will focus on the finite-difference time-domain (FDTD) numerical method. Also called Yee's method after the inventor of the method, applied mathematician Kane Yee, FDTD can be applied to calculate reflectance, transmission, diffraction, interference, and absorption of different structured or unstructured materials; study the response to different polarizations and wavelengths of light; and record movies to visualize how light travels through the materials in real time. FDTD was first introduced in 1966 (Yee, 1966), and more efficient features and algorithms have been developed over the past five decades (Yee, 1966; Gedney, 2011; Wan et al., 2017), including parameter sweeps over many features of interest. FDTD is now a mature and widely-implemented method of simulation available in well-documented commercial and open-source programs. Compared to many other common numerical methods, FDTD simulations are particularly well suited for researchers who wish to (i) conduct broadband simulations (in which light sources contain a large wavelength range) and (ii) investigate the behavior of light over time, from when it is emitted from the source through its interaction with the object and beyond.

A common workflow for FDTD is shown in schematic form in Fig. 1. Typically, when researchers observe an optical effect of interest in an organism, a portion of the organism is dissected and imaged using sophisticated microscopy (e.g., transmission electron microscopy (TEM) in Fig. 1A; more examples are discussed in Section 4.1.2). The structure is represented in a simulation domain (Fig. 1B, Sections 4.1.3–4.5). Then, the researcher can implement FDTD simulations to assess how light interacts with that structure and analyze their results (Fig. 1C, Sections 4.6–4.9).

FDTD simulations operate by solving for how light, an electromagnetic wave, propagates through a user-defined structure in a medium (such as a bird feather in air, shown schematically in Fig. 1). Under the hood, the software is solving a modified form of Maxwell's coupled differential equations — the famous equations in optics describing the propagation of electromagnetic waves in media with different physical characteristics (Jackson, 1999) — in a stepwise manner (alternating between solving for the electric or magnetic field at each discrete time point and spatial location). The simulation volume is divided into a grid, which defines the discrete spatial locations, and the borders of the

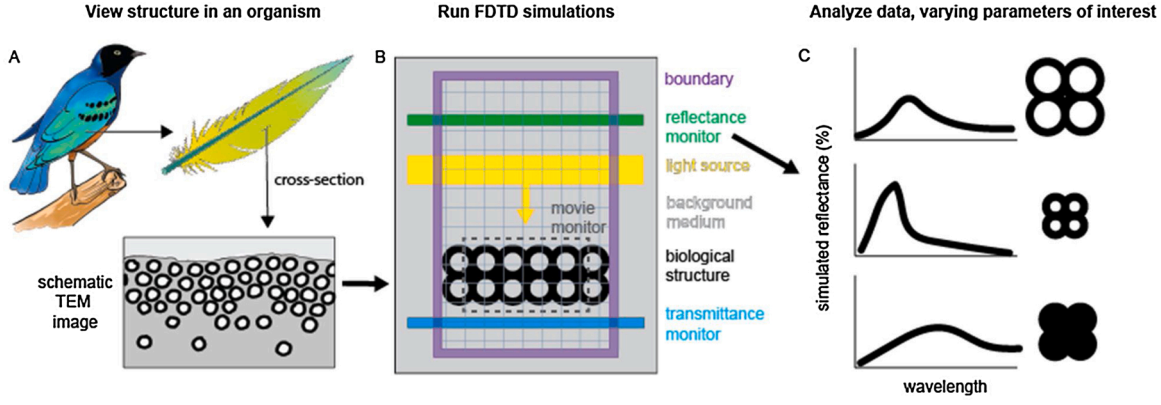

Fig. 1. Schematic overview of the FDTD workflow. **(A)** First, the optical effect is observed, such as a bird's colors. A portion of a feather is removed, prepared for microscopy, and imaged. For the example shown, sample preparation involves embedding the piece of the feather into a resin, producing a thin (< 100 nm) slice, and placing it on a conducting grid. Transmission electron microscopy (TEM) is used to identify hollow melanin-containing features called melanosomes within the bird feather. **(B)** Microscopy images can then be imported into finite difference time domain (FDTD) software, or the user can draw an approximation or idealized form of the structure. The user places and assigns properties to each of the elements of the simulation, and the simulation is run until a user-defined end point to calculate the interaction of light with the user's structure of interest. A variety of monitors can be employed to record the electromagnetic field at specific time points, locations, and frequencies. The monitors depicted in the schematic collect reflectance and transmission data and record a movie of light interacting with the structures. **(C)** The simulation results can be graphed and analyzed. Here, artistic renditions depict reflectance spectra for different manifestations of the melanosomes in bird feathers, where melanosomes are varied by size and whether or not they are hollow. Artwork in (A) is by Kay Xia (bird) and Ana Kimber (feather and TEM schematic).

domain are assigned appropriate boundary conditions; the user specifies a light source and light detectors ("monitors"), which collect the light in discrete time steps over the entirety of the simulation time. Once the simulation has terminated, data from the monitors — such as reflectance and transmission — can be extracted and visualized, depending on the question of interest.

FDTD simulations are flexible, with the advantage that researchers can conduct parameter sweeps to explore the effects of modifying characteristics of interest (Fig. 1C), such as a structure's size or refractive indices; the addition of layers to a repeating or hierarchical structure; the refractive index of the medium (e.g., air, water, or other); or aspects of the light source. This gives researchers the opportunity to investigate the consequences of many variations and combinations that would be impossible or extremely difficult to perform in the natural world or with synthetic analogues. For example, what color would a duck's iridescent green head be if the melanosomes (melanin-containing organelles) in its feathers were a little longer or shorter? Do the structures result in "optimum" brightness, or could a large range of dimensions provide the same results? What do those conclusions tell us about sexual selection in ducks? What palette of greens can we produce for commercial paints based on these principles? In addition to wrangling ducks in the wild, researchers can better understand the natural world with FDTD.

This methods primer begins with a broad literature review of FDTD applied to questions in biology and biologically-inspired engineering (Section 2). As FDTD is becoming more common in these fields, it is impossible to provide a comprehensive discussion of all relevant papers; the aim here is to cast a wide net so that interested readers can pursue specific topics in more detail. Section 3 is designed for readers interested in understanding FDTD in the context of other optical simulation tools and/or in determining whether or not FDTD is the right approach for their questions (for a decision flow chart, see Fig. 2). Section 4 provides a

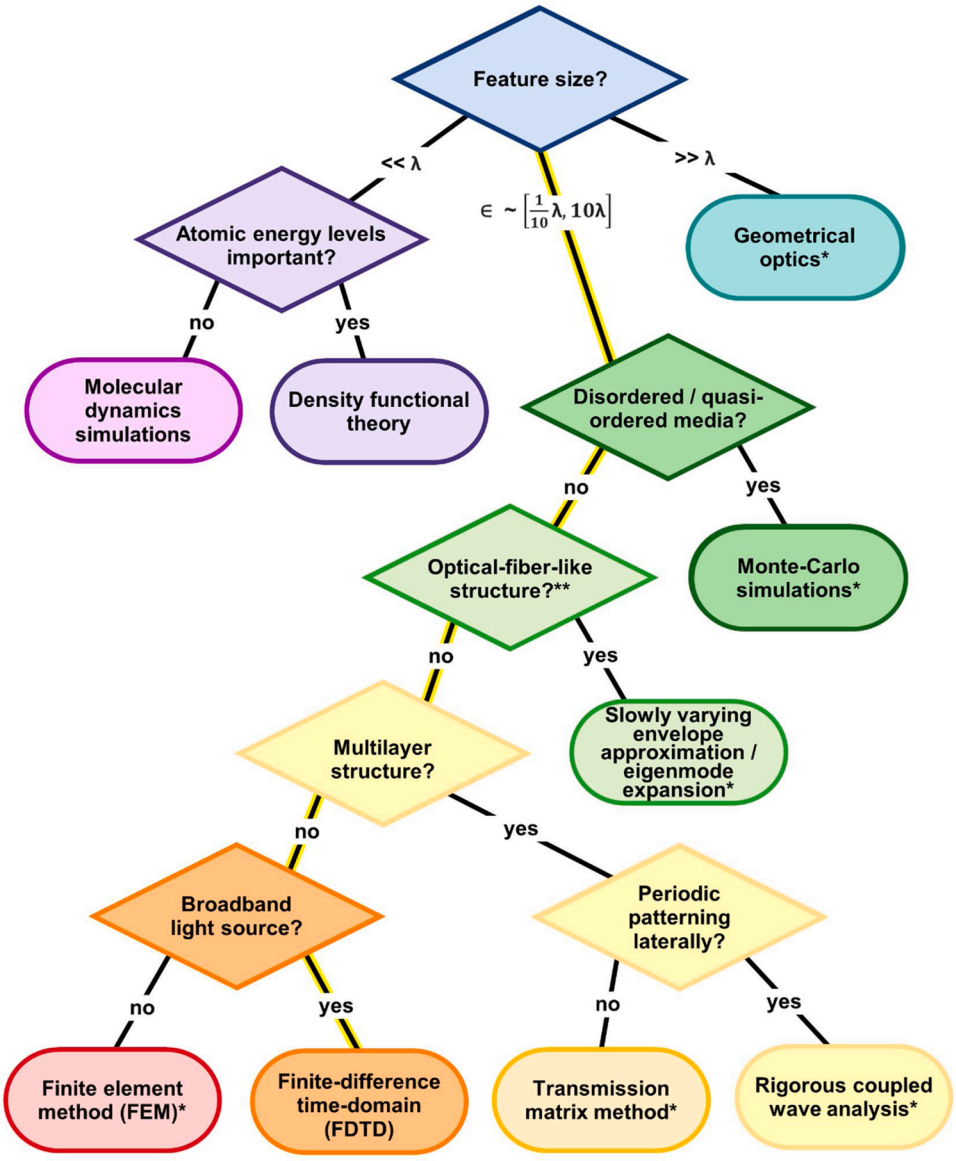

Fig. 2. Flow chart suggesting when to select FDTD among other common optical simulation techniques. Diamonds represent decision points, while ovals are the simulation techniques. FDTD is reached by following the yellow-highlighted path to the orange oval at the bottom. As a rule of thumb, FDTD is most appropriate for structures consisting of feature sizes approximately a tenth of a wavelength to ten wavelengths ($\in [1/10\ \lambda, 10\lambda]$). Well below this ($<<\lambda$), molecular motion and quantum effects become important, which are not included in FDTD. At larger length scales ($>>\lambda$), simulation times become intractable, and geometrical optics is more appropriate. Note that FDTD and FEM can, in principle, be applied to most of the situations in the flowchart (methods labeled with asterisks, *); however, FDTD and FEM are likely less efficient than the methods tailored to the special cases. The methods presented here are not exhaustive, but provide general guidance. See Section 3 for discussion of other methods (e.g., finite element time-domain (FETD)). A researcher may choose to perform multiscale modeling, in which case multiple techniques would be useful.

* FDTD (and FEM) can be used, but they are typically less efficient than the specialized method.

** The cross-section of the structure is almost constant in the direction that light is travelling. Slowly varying envelope approximation (SVEA, utilized in the beam propagation method) requires that (i) variations occur on a length scale >> λ and (ii) the refractive index contrast is small. Eigenmode expansion is more rigorous and, thus, more general.

primer of the FDTD method and how to implement it, specifically focusing on the software *Lumerical FDTD*. For readers who wish to conduct FDTD simulations on a particular organism, we suggest reading (i) the papers referenced in Section 2, (ii) *Lumerical*'s online tutorials targeted for the structure of interest, (iii) tutorials from other available open-source and licensed FDTD software, and (iv) other overviews of FDTD (Gedney, 2011; Sullivan, 2013; Wan et al., 2017). Sections 2 and 3 can be skipped or saved for later for readers wishing to immediately immerse themselves in the FDTD technique theory and implementation.

2. Example Applications of FDTD to Biology

Natural scientists use FDTD simulations to precisely characterize the physical basis of color and other light-dependent phenomena. FDTD is especially useful when nano- and micro-scale structures that reflect, transmit, and scatter light are involved, such as those shown in Fig. 3 for the moss (Chandler et al., 2015) and beetle (Wilts et al., 2018b). By understanding the physical basis of optical adaptations, we can make strides in three areas: exploratory science (Section 2.1), evolutionary theory (Sections 2.2, 2.3), and bio-inspired technology (Section 2.4).

First, micro- and nano-scale optics in nature are a frontier of research, akin to the deep sea or dense forest. Researchers can use FDTD with microscopy and other tools to explore fundamental biodiversity at small scales, opening up new research questions in organisms from peacocks to peacock spiders (Section 2.1). Second, we learn more about evolution by understanding the physical, proximate cause of biological optical adaptations. FDTD can help scientists understand sexual selection as it can be used to analyze the role of pigments and structures in colorful signals (Section 2.2) and evolutionary innovation across environmental conditions, from photosynthesis in the shade to deep-sea abyssal arms races between predators and prey (Section 2.3). Third, FDTD simulations allow researchers to characterize natural innovations, and design and test technologies inspired by nature — "bioinspired" technologies including, for example, solar cells, light sources, sensors, devices for thermal management, and more (Buss, 2009; Dou et al., 2021; Kim et al., 2012; Kolle et al., 2013; Muehlberger et al., 2021; Pris et al., 2012; Sandt et al., 2018; Seo and Lee, 2017; Stratakis et al., 2020; Zhang et al., 2020; Zhao et al., 2011). Biodiversity is important not only aesthetically and ecologically but also as a source of innovation (Section 2.4).

2.1. Exploring the physical basis of structural color

FDTD, at the most basic level, helps researchers understand experimental data and evaluate hypotheses regarding the nature of structural color and other optical effects at the micro and nano-scale.

Birds have some of the most dazzling color displays on Earth, and researchers have used FDTD in combination with other tools to explain what makes bird feathers shine. In particular, FDTD is often applied to (i) identify which structural features within a bird feather are most important for color and (ii) compare them to other possible structures in order to understand whether the structures used in nature are particularly well-suited for an optical effect. Parameter sweeps in FDTD were employed to determine that common magpie's (*Pica pica)* feathers vary in color from blue to purple-to-green due primarily to the diameter and hollowness of melanosomes embedded in stacks in the keratin matrix (Stavenga et al., 2018). Mallard ducks (*Anas platyrhynchos*) have blue feathers in their wings, and males have green heads, both of which arise from multilayered melanosome stacks; using FDTD, the researchers demonstrated that the multilayer period and cortex thickness, rather than spatial arrangement of melanosomes, were more important for color (Stavenga et al., 2017). Some birds (wild turkeys (*Meleagris*

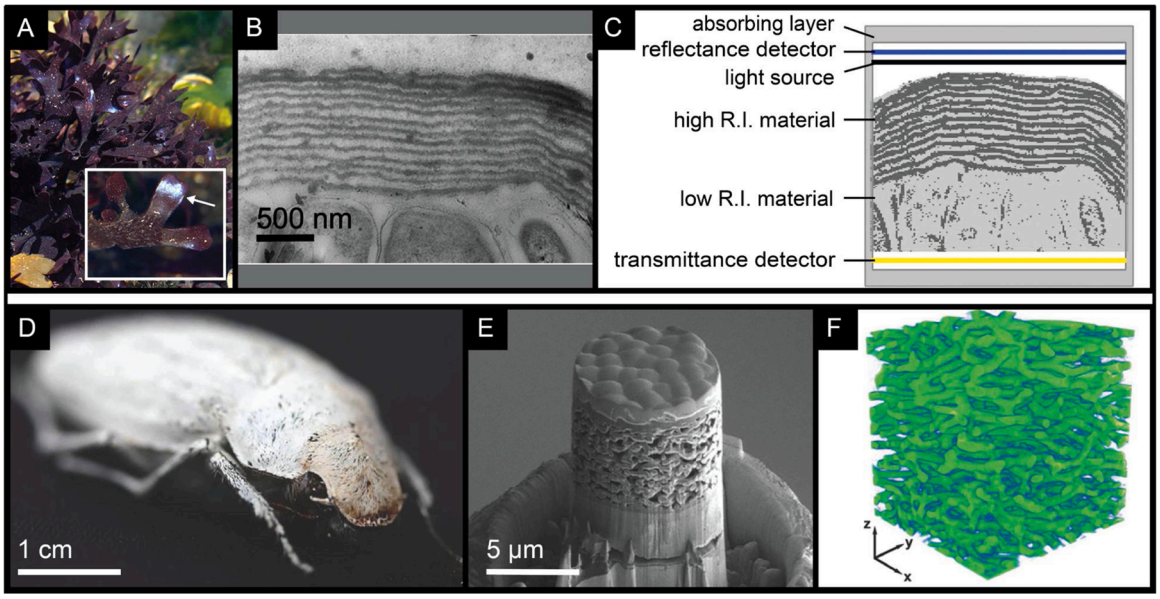

Fig. 3. Researchers can import 2D or 3D microscopy or tomography data into FDTD simulation software. **(A-C)** Irish moss (*Chondrus crispus*) owes its structural blue color to multilayered cuticle structures and water, possibly an adaptation to block UV light (Chandler et al., 2015). **(D-F)** White beetles *Cyphochilus* sp. have randomly structured 3D media to give the highest reflectance for the smallest amount of materials, possibly an adaptation for camouflage among white fungi in a shady environment (Wilts et al., 2018b). **(A)** A photograph of Irish moss, *Chondrus crispus,* shows intense blue color at the tips of the fronds (photograph by Chris J. Chandler). **(B)** Transmission electron microscope (TEM) image of a cross section of cuticle at the tip of a *Chondrus crispus* frond. **(C)** Schematic of FDTD simulation in the software *Lumerical*, showing a binary representation of the TEM image in (B) with refractive indices assigned to each shade of gray: light cellulosic materials (n = 1.46); dark-stained material (n = 1.55); and a boundary box filled with water (n = 1.33). Absorbing boundary conditions are applied on all sides of the computational domain. **(D)** A photograph of the beetle *Cyphochilus* sp. with brilliant white coloration (photo by Charly Rappo). **(E)** Scanning electron microscope (SEM) image of a pillar obtained from a beetle scale through focused ion-beam (FIB) milling. **(F)** 3D reconstruction of the interior of a beetle scale, 7 μm^3, obtained by cryo-ptychographic X-ray tomography (cryo-PXCT) for FDTD simulations. Figure credits: **(A-C)** (Chandler et al., 2015), reproduced under terms of the CC-BY-4.0 (creativecommons.org/licenses/by/4.0/), Copyright 2015, The Authors, Published by Springer Nature; **(D-F)** (Wilts et al., 2018b), reproduced under terms of the CC-BY-4.0 (creativecommons.org/licenses/by/4.0/), Copyright 2018, The Authors. Published by WILEY-VCH Verlag GmbH & Co. KGaA, Weinheim.

gallopavo) and violet-backed starlings (*Cinnyricinclus leucogaster*)) evolved hexagonal arrays of hollow, rather than solid, melanosomes. By employing FDTD to compare different types of melanosomes, the authors of the study concluded that hollow melanosomes can produce a wider array of colors while maintaining the thermodynamically favorable close-packed arrangement of solid melanosomes (Eliason et al., 2013). Dabbling ducks (tribe Anatini) produce iridescent colors through a keratin thin-film and melanosome lattice; researchers used FDTD to simulate the many possible configurations of the two-part photonic heterostructures, thereby showing that birds use only a small, energetically-stable subset of those that are theoretically possible (Eliason and Shawkey, 2012).

FDTD was also applied to study the cylindrical pigment granules in the pheasant *Polyplectron bicalcaratum* and pigeon *Patagioenas fasciata* (Eliason and Shawkey, 2014); these pigment granules form a gradient of refractive indices to selectively block certain wavelengths of light and enhance others. Male peacocks (*Pavo cristatus*) owe their brilliant colors to two-dimensional photonic crystals composed of melanin granules, keratin, and air in their blue necks, breast feathers (Freyer et al., 2019), and green eyespots on their tails (Wang et al., 2020). By pairing FDTD with simple multilayer modeling and experimental measurements, the researchers showed that simple multilayer modeling was adequate to explain the iridescence of peacock feathers (Freyer et al., 2019).

Though significantly smaller than birds, insects and arachnids present an incredible variety of photonic structures, including those that produce brilliant structural colors. The Australian peacock spiders (*Maratus,* Salticidae), although perhaps less well known and tinier (~2-7 mm across) than their bird namesake, are no less colorful and elaborate in their mating displays. By slicing open specimens and using SEM, scientists identified a range of internal microstructures; next, they used FDTD simulations to help identify that flat, ordered gratings are responsible for iridescent rainbow colors in peacock spider *Maratus robinsoni*, while its cousin *M. nigromaculatus* gets its angle-independent blue color from dense, curved, disordered gratings (Wilts et al., 2020). Researchers have also applied FDTD to explain the stunning photonic architecture of beetles, weevils, and their relatives. The Brazilian diamond weevil (*Entimus imperialis*) has concave green spots in its elytra patterned by scales with 3D photonic crystals; FDTD helped demonstrate that the highly directional reflectance of the crystals becomes angle-independent green due specifically to the concave pits. The color is thought to serve as camouflage, a close match to background foliage (Wilts et al., 2012). The longhorn beetle (*Sulawesiella rafaelae*) varies in color from yellow to gold to blue-green as the multilayered architecture within their scales varies from ordered to disordered; the authors used focused ion beam in conjunction with scanning electron microscopy (FIB/SEM) to visualize microstructures within the scale cross section and FDTD to construct, and test the reflectance from, idealized 3D scale forms (Bermúdez-Ureña et al., 2020). Additionally, ultra-white beetles have evolved morphology that gives the highest known white reflection for the minimum use of materials through randomly structured 3D media (Wilts et al., 2018b). The researchers used FDTD to simulate the reflectance from digitally altered structures of the beetle scale, thereby showing that any change in the realistic parameter space resulted in lower reflectance or the need for heavier/thicker materials (Wilts et al., 2018b).

Butterflies are some of the best-studied bearers of structural color, and scientists have used FDTD together with microscopy and spectroscopy to disentangle which structural features are most important for producing any given color (Márk et al., 2019). The Green Hairstreak butterfly, *Callophrys rubi*, has 3D gyroid cuticular structures; researchers employed FDTD to confirm that these structures (i) act as a photonic crystal to produce an omnidirectional green color, likely for camouflage, and (ii) produce scattered light that is elliptically polarized, potentially as a mating signal (Michielsen et al., 2010). FDTD was used to identify steep ridges and expanded trabeculae of the scale as the most important structures for decreasing reflectance in many species of super black (reflectance $< 0.5\%$) butterflies (e.g., *Catonephele numilia* or *Trogonoptera brookiana* males). FDTD also allowed the researchers to quantify the relative contributions of absorption (by melanin) and scattering (from chitin) versus total scale absorption (Davis et al., 2020a). Scientists have also gazed across millenia to compare gold-colored insects preserved in amber to their living relatives (D'Alba et al., 2019). The authors analyzed extinct micromoths (Lepidoptera: Micropterigidae, 15 millions years old) and their living relative *Micropterix calthella,* as well as extinct springtails (Collembola: Tomoceridae, 99 million years old) and their living relative *Tomocerus vulgaris*: FDTD was implemented to show that both extant and extinct animals used "nearly identical" crossribs and diffraction gratings to produce gold color (D'Alba et al., 2019).

Beyond birds and insects, flowers have offered a fruitful domain for employing FDTD simulations to isolate the structural basis of flower color and iridescence. In California poppies (Eschscholzia californica), FDTD was used to identify two distinct optical phenomena taking place within the petals: (i) the petal surface produces specular reflection and (ii) a microlens at the epidermal cell tip focuses light onto the pigment-containing plastids (Wilts et al., 2018a). The authors also used FDTD to demonstrate that these effects were largely invariant with refractive index across a naturally-relevant range. Similarly, FDTD simulations were used to confirm that disordered wax platelets in the purple heart flower *Tradescantia pallida* are responsible for producing a golden shine (van de Kerkhof et al. 2020). In a study of many flower species, researchers simulated flower petal micro-gratings with various amounts of disorder to demonstrate that the "blue halo" produced by these gratings is not significantly affected by disorder within the observed range (Moyroud et al., 2017).

Structural color has also been identified in some fruits, including the famous Pointillist blue in the marble berry *Pollia condensata* (Vignolini et al., 2012). FDTD was applied to study the structurally colored paper thin silver-dollar fruits of the honesty plant *Lunaria annua*. The scientists used FDTD to identify key hierarchical features producing the silvery-white color: two thin (~310 nm thickness) layers of tube-shaped cells with a hollow center create thin-film interference (Guidetti et al., 2020). FDTD confirmed that because the cells vary in thickness, each region selectively reflects a different color. Taken together, the whole fruit reflects a broad range of colors to produce a highly-reflective silvery white.

Some bacterial communities, such as the hexagonal assemblages of the bacteria *Flavobacterium* IR1, also display structural colors. The 3D spatial arrangement and orientation of bacterial colonies is interesting but difficult to measure using invasive methods such as electron microscopy due to distortions during preparation. Researchers demonstrated that data from optical goniometry, by which they collected angle-resolved reflectance spectra from living bacterial communities, can be used to determine the spatial arrangement and orientation of bacteria from structural color appearance alone. The authors used FDTD to confirm this result by investigating the optical effects of varying (i) the orientation of the bacteria relative to the direction of incident light and (ii) the degree of disorder in the assemblage (Schertel et al., 2020). To investigate disorder, the authors introduced deviations from a perfect lattice structure into the simulated geometry.

Diatoms, a common unicellular photosynthetic algae, efficiently harvest solar energy thanks to their silicate cell walls with hierarchical nano- and micro-structures. Researchers used FDTD along with experimental measurements of absorption to show that the structural features, known as frustules, on diatom skeletons strongly enhance visible light absorption (Chen et al., 2015). In a subsequent study, researchers used microfiber spectroscopy (by collecting transmitted light beneath the specimen which was illuminated from above) to measure the absorption spectrum of the skeleton between 400 and 500 nm. They performed FDTD simulations to show that the particular photonic crystalline features of the diatom's skeleton enhance absorption of light near 420 nm, therefore enhancing their photosynthetic efficiency (Yoneda et al.,

2016).

2.2. Evolutionary effects, and production of, sexually-selected signals

FDTD allows researchers to more thoroughly characterize colorful signals, therefore helping to provide insights into the working of sexual selection. Some ornate animals orient themselves in specific directions toward potential mates, and FDTD has helped characterize the micro- and nano-scale basis of these directional optical adaptations. Stunning examples of this type of display are performed by birds-of-paradise (Frith and Frith, 1988; Laman and Scholes, 2012). Sparkling, directionally-variable feathers in the bird-of-paradise Lawes's Parotia (*Parotia lawesii*) are produced by layers of melanin rods and keratin embedded in feathers with a boomerang-shaped cross section (Wilts et al., 2014). The authors used imaging scatterometry to show that *Parotia lawesii* feathers vary sharply in color across viewing angles, the feathers directionally reflect light at discrete angles, and that the reflectance depends strongly on polarization; next, they applied FDTD to a grayscale TEM cross-section of the feather to confirm that the feathers' boomerang-shaped microscale anatomy (in combination with the broadband absorption provided by melanin) produces all of the experimentally measured features (Wilts et al., 2014).

Similarly, during mating displays, many species of jumping spider orient themselves directly in front of females to show off their brilliant colors (Echeverri et al., 2017; Girard et al., 2011; Otto and Hill, 2013). Some male peacock spiders (*Maratus* spp.) have super-black abdomens, exhibiting $< 0.5\%$ reflection when a viewer (female spider) is directly looking at them. This produces an optical illusion by which nearby colors appear brighter (McCoy et al., 2019). FDTD simulations with parameter sweeps were employed to test the optical effect of varying microlens height, radius, shape, and packing arrangement (Fig. 5). This revealed that the microlenses are (roughly) optimally sized and shaped to absorb as much light as possible and reflect the least (McCoy et al., 2019). Sexually-selected birdwing butterflies of the genus *Ornithoptera* vary dramatically in color patterns even between closely related species. In a study which used scatterometry and FDTD, researchers identified the mechanisms of color production, and drew three interesting conclusions about sexual selection across a genus (Wilts et al., 2015). First, the specific methods of color production — chirped multilayer reflectors and spectral filtering by a group of yellow (papiliochrome) pigments — strongly correlate with taxonomic distribution (Wilts et al., 2015). Second, the butterfly's signals are carefully tuned through a combination of pigment and structure to generate a broad-angled UV and yellow-green colored signal (Wilts et al., 2015) — providing an example of a "nonspectral" color (i.e., mix of nonadjacent long and short wavelengths, akin to purple, rather than a color produced by adjacent wavelengths) in visual display. Third, the colorful signals appear to be tuned to the specific sensitivities of butterfly cone receptors (Wilts et al., 2015).

FDTD can also be used to study the emergence of structural color over an organism's lifetime, which, in combination with genetics, can tell a rich developmental story. Consider the blue-tailed damselfly (*Ischnura elegans*). Males change from green to blue as they mature, and females begin life as red or violet but age into the same blue color as adult males, potentially a technique to avoid harassment (Henze et al., 2019). Researchers used FDTD to show how the physical basis of color changes over male and female damselfly's lives (performing simulations based on structures obtained from dissected samples at different levels of maturity). Color changes arise from (i) the development of a distal layer of densely packed nanospheres in a watery matrix in the epidermis, in addition to existing nanospheres and (ii) changes in the pigment composition of the nanospheres, therefore offering guidance for geneticists to help identify candidate genes that regulate color changes with maturity (Henze et al., 2019).

"Honest signalling theory" is the idea that mating displays evolve to be colorful and elaborate as an honest signal of quality, by which potential mates can select genetically fit individuals. Carotenoid pigments—which make many birds appear red, orange, and yellow—are an archetypal example of honest signalling (Weaver et al., 2018). FDTD helped show that some carotenoid-colored male birds fly under false colors. Red, orange, and yellow male tanagers (*Ramphocelus*spp.) evolved microstructures which reduce surface reflection and enhance light-pigment interactions, contributing to a richer color without requiring more carotenoid pigments (McCoy et al., 2021).

2.3. Evolutionary innovation across environmental conditions

In low-light conditions, aquatic ecosystems, and other environments, many organisms have evolved fitness-increasing strategies to manipulate light. Numerous shade-dwelling plants possess iridoplasts (chloroplasts in the epidermis) with highly organized thylakoid membranes. To investigate whether this organization plays a role in photosynthesis, researchers used electron microscopy to obtain the ultrastructure of iridoplasts from leaves of a *Begonia* hybrid (*B. grandix* X *B. pavonina*), the transmission matrix method for multilayers to calculate the reflection spectrum from the obtained structure, and FDTD to simulate the electromagnetic field profile within an iridoplast under white light illumination (Jacobs et al., 2016). The authors found that the iridoplasts consist of ~3 thylakoid membranes in ~40 nm thick grana, which are themselves regularly spaced with a separation of ~100 nm. Optical modeling showed that this arrangement increases photosynthetic light capture for these plants' low-light environments through a mechanism known as the "slow-light" effect, particular to photonic crystals, wherein light at certain wavelengths (specifically in this case, the low intensity bluer light that makes it through the dense canopy) is halted to a standstill within the structure, increasing its absorption (Jacobs et al., 2016).

Fish are masters of underwater vision, and they have evolved optical structures to assist vision in challenging conditions. Peters's elephantnose fish (*Gnathonemus petersii*) have special light collectors on their retina to see through cloudy water; researchers used FDTD to show that four layers of guanine crystal lamellae enhance light collection by concentrating light within the crystal structure on the light-sensitive outer segments of cones (Kreysing et al., 2012). Inspired by this work, the same authors and other collaborators conducted a large suite of FDTD simulations to analyze the functions and effects of "tapetal cups" (adaptations of the retina) across the Teleost infraclass; they found many structural features which enhance light intensity, such as multilayer reflectors made from guanine, uric acid, or pteridines (Francke et al., 2014).

While some organisms manipulate light to see, others manipulate it to remain unseen. These adaptations are common in the deep sea. In the mesopelagic, hatchetfish (*Argyropelecus* sp.) have two-layered reflectors consisting of guanine platelet stacks, one flat and one diamond-shaped, allowing the hatchetfish to remain camouflaged when illuminated with either direct or diffuse light as light is reflected across a semicircular area instead of directly back towards the source (Rosenthal et al., 2017). The copepod *Sapphirina nigromaculata* also has guanine platelet stacks, hexagonal in shape, which underpin its tunable structural color (from achromatic to yellow, red, and blue likely either for display to conspecifics or to remain unseen from predators); scientists used FDTD to calculate transmitted and reflected light across a range of inter-platelet distances (0-100 nm), showing that the distance between guanine plates is a key driver of the color (Kimura et al., 2020). The bioluminescent photophores on the eyes of the midwater squid *Galiteuthis* help camouflage the squid from the view of predators (below the squid). FDTD simulations showed that "leaky" multilayer light guides reshape the electromagnetic field profile of the squid bioluminescence to tailor it to the surrounding radiance (Holt and Sweeney, 2016). Deeper in the ocean, some fishes have evolved skin that reflects $< 0.5\%$ of light by tightly packing ellipsoidal melanosomes together. By varying the size and aspect ratio of the simulated melanosomes, the authors of the study

revealed that the ones matching those of deep-sea fish melanosomes minimize reflectance (Fig. 4, (Davis et al., 2020b)).

Some organisms use their environment to produce particular colors or light-harnessing adaptations. The intertidal red algae Irish Moss (*Chondrus crispus*, shown in Fig. 3) displays a striking blue color at the thallus tip (Chandler et al., 2015). FDTD was applied to confirm that the blue color is structural and results from stacked lamellae within the thallus tip (Chandler et al., 2015), and a followup study was conducted to find that this structural color in marine algae varies alongside environmental conditions, such as water turbidity and radiation intensity (Chandler et al., 2017). In algae, therefore, structural color is thought to be an environmental adaptation rather than an adaptation for signalling (Chandler et al., 2017). Similarly, researchers are continuing to investigate whether structures in other organisms that have been shown to have optical effects in the lab are purely incidental or play an optically functional role, such as the optical fibers of deep-sea sponges (Aizenberg et al., 2004) and beetles that change color at higher humidities when their porous exoskeleton becomes wet (Mouchet et al., 2014; Rassart et al., 2009). FDTD can be applied to understand mechanisms and answer many questions, but it also opens the doors to biological mysteries that can be further explored through a combination of tools.

2.4. Biomimicry and bioinspired design

In addition to helping provide insight into the biological world, FDTD can be used to guide the design of bio-inspired materials. Butterflies are a treasure trove of inspiration. Consider the moon satyr butterfly (*Pierella luna*), which appears brown under normal conditions but flashes a colorful spot at a low viewing angle. Its wingspot displays angle-dependent color that changes from blue to red as the angle of observation increases, a diffraction of light in the opposite sequence than is normally observed (Vigneron et al., 2010). The butterfly's reverse diffraction was an intriguing mystery to researchers, who hypothesized that it arose due to the double grating structure on the butterfly's curving scales (which they observed with SEM). FDTD simulations validated this idea and allowed the researchers to conduct parameter sweeps to determine what happens if the spacing of the grating changes. Guided by these observations and simulations, the authors designed and fabricated artificial diffraction gratings in various materials, showing the same reverse diffraction as that of *P. luna* (England et al., 2014).

Similarly, FDTD allowed researchers to explore the optical consequences of varying the spacing, size, and symmetry of the nanostructures responsible for the metallic blue reflection of the *Morpho* butterfly; they found the spacing of layers within the scale, but not their width or thickness, can shift the reflection peak maximum by up to 25 nm and determines the presence of a secondary reflection peak centered around 700 nm (Steindorfer et al., 2012). These *Morpho* butterfly scales have inspired the creation of biomimetic sensors and absorbers (Butt et al., 2016). Super black butterflies (first identified in species *Papilio xuthus* (Vukusic et al., 2004)) evolved light-trapping scales, structures which inspired new ultrathin absorbing carbon film technology (Zhao et al., 2011). Likewise, the scarab beetle *Chrysina gloriosa* has green and silver stripes due to concave polygonal cells (with mirror-like reflections) which may inspire technological improvements on classic convex cells used in wavelength-specific micromirrors (Agez et al., 2017).

Fireflies send bioluminescent sexual signals and are thus incentivized to increase light transmission from their "lantern" to the outside world (Bay et al., 2013). Researchers used FDTD to characterize the ordered nanostructures on the firefly cuticle, which boost the sexual signal by increasing transmission through ordered longitudinal ridges on the cuticle. These ridges, in turn, inspired novel, efficient curved LED lenses featuring similar ridges (Kim et al., 2012).

Biologically-inspired optics are not restricted to animals. A tropical fruit, *Margaritaria nobilis*, has a concentrically-layered photonic structure which inspired researchers to design tunable elastic fibers which can adjust the reflected wavelength by more than 200 nm (Kolle et al., 2013). These fruit-inspired tunable fibers have recently been applied to medical bandages to sense sub-bandage pressure, with a view towards improving patient outcomes (Sandt et al., 2018).

The examples presented throughout Section 2 demonstrate that

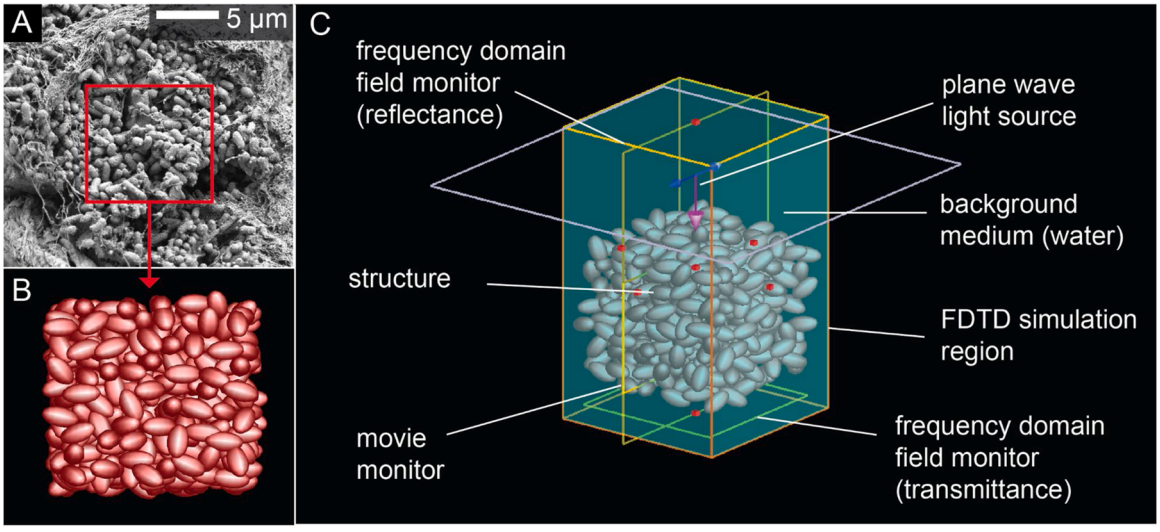

Fig. 4. Overview of a simulation using disordered melanosomes of super-black fish (*Oneirodes* sp.) skin as an example. **(A)** SEM image of the melanosomes from the outer layers of the epidermis of super-black fish skin, which reflects as little as 0.05% of incoming light. **(B)** Geometry used for FDTD simulations, drawn by creating a random packing of ellipsoids with an aspect ratio of 1.75 and a sphere-equivalent diameter of 700 nm. The background medium (black) is assigned a refractive index of 1.334, that of the fish's water environment. **(C)** Screenshot of FDTD simulation in *Lumerical*. A plane wave light source is placed above the structure, with the purple arrow showing the direction of light travel and the blue arrows indicating the (linear) polarization of the electric field (blue and purple arrows are faint lines centered in the X-Y plane and above the fish melanosomes in the Y-Z plane). Frequency domain field profile monitors capture electromagnetic waves that emerge above (reflectance) and below (transmission) the structure, while the 2D movie monitor shows the light as it propagates through the structure, in the indicated plane. The boundary conditions are perfectly matched layers on the top and bottom X-Y planes and periodic on all four side planes (X-Z and Y-Z). This figure is based on analyses from Davis et al. (2020).

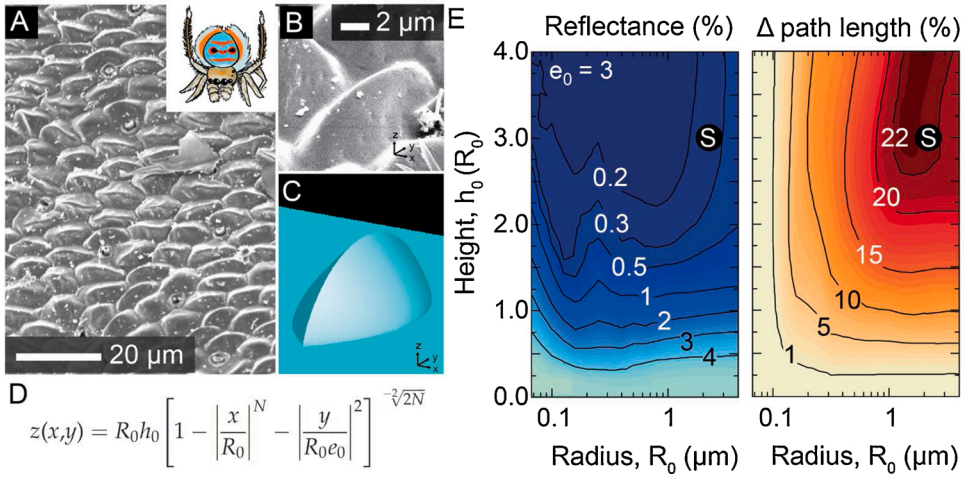

Fig. 5. FDTD analysis allows for parameter sweeps, such as in this simulation of super black peacock spider (*Maratus speciosus*) cuticle. By varying the size and shape of cuticle bumps (simulated by a scripted equation), data on reflectance and path length could be gathered across a parameter space. **(A)** SEM image of cuticle from *Maratus speciosus* showing microlens array; inset illustration by Kay Xia. **(B)** Close-up view of a single microlens. **(C)** Screenshot of the custom superellipsoid created in *Lumerical FDTD* to approximate a peacock spider cuticular microlens. **(D)** Equation for a superellipsoid in (C) used to approximate the microlenses in a peacock spider simulation; z is its height at spatial position (x,y), *R0* is its radius on the short axis, *e0* is elongation, *h0* is height, and *N* determines the shape of the superellipsoid (2 corresponds to an ellipsoid and 1 is near-pyramidal in the x-direction; $N = 2$ in.(C)). **(E)** Parameter sweeps over reflectance (left) and change in path length through a melanin layer (right) show that the spider (circle with S) is sitting at a rough optimum for maximal path length and minimal reflectance. All data re-plotted from McCoy et al. (2019).

FDTD can be used for fundamental biophotonics research, evolutionary analyses, and bio-inspired design, among numerous other purposes.

3. Choosing the Right Optical Simulation Technique

It is important to note that while the FDTD method is useful for researchers interested in biological optics, it is not always the right tool. This section compares FDTD to several alternative simulation tools and available software, though it is by no means exhaustive. As mentioned in the introduction, readers who wish to learn how to implement FDTD can skip to Section 4. Readers who would like more information on the variety of computational methods available should look to computational electromagnetics textbooks (Rylander et al., 2013; Sheng and Song, 2011) and lectures.

Researchers can choose from a sometimes-overwhelming number of simulation techniques, possible implementations, and software. A good place to start is with a quick search of the literature for simulations involving similar structures to the one of interest. More broadly, when selecting a simulation method, critical considerations include (i) optical effects of interest (e.g., reflectance or fluorescence), (ii) length-scales and time-scales involved, (iii) the users' comfort level with programming versus graphical user interfaces (and ready-to-use versus self-written software), and (iv) computational resource requirements. Fig. 2 shows a flow chart for when to select which technique, keeping in mind that a combination of techniques (multiscale modeling) may be necessary or interesting to consider. More details on the selection are provided in the sub-sections that follow.

Even if FDTD is the right tool, there are some situations which are particularly challenging and will take significantly, perhaps prohibitively, longer to run than others (because FDTD is ultimately limited by computer memory). Longer runtimes for similar settings are encountered when simulations contain structures that: (i) are significantly larger than the wavelengths being studied and cannot be accurately modeled with a much smaller unit cell or representative volume element; (ii) vary in size over orders of magnitude (e.g., having microscopic pores (~10^-6 m) on a millimeter sized object (~10^-3 m)); (iii) consist of materials with high absorption or dispersion (one or more of the materials properties such as refractive index or absorption exhibit large variations with wavelength within the wavelength range of interest); or (iv) exhibit substantial nonlinear optical responses (when there are significant contributions to the optical response not only from the amplitude of the electric and magnetic fields of the electromagnetic waves but also from the square of the amplitude, cube, or higher-order terms). In those cases, specific details of the algorithms (e.g., the ways in which the structure meshing, differential equations, and electromagnetic fields are encoded) can be crucial to ensure reasonable run times while achieving sufficient accuracy.

3.1. Size Scales of Interest and Appropriate Methods

Large structures require large simulation domains which lead to longer computational times. Therefore, FDTD is best used when the domain size can be smaller than tens of wavelengths across for 3D simulations and hundreds of wavelengths for 2D simulations (Kimmel and Christensen, 1992). For structures with all feature sizes orders of magnitude larger than the wavelengths of light involved, such as a fish eye (Jagger, 1992), geometrical (or ray) optics is the best tool rather than FDTD. Geometrical optics simplifies light as straight lines (rays), and simulations require significantly less computation time and resources than FDTD or other methods that include more physical details.

When length scales of objects become closer to the wavelengths of light being studied (often ~400-700 nm light in biological studies), the ray optics approximation fails because it does not account for important phenomena that occur at these size scales, such as diffraction and interference. In such cases, researchers should use simulation methods that rely on full-wave equations of electromagnetism (such as FDTD and others, described below). Such methods take into account the oscillations of both the electric and magnetic fields and their effects as they interact with electrons on the materials they encounter; that is because these methods encode Maxwell's equations, the constitutive relations, and the simulation boundaries— albeit in different ways (Burger et al., 2005). Though any of these methods can be used in principle, they may have advantages and disadvantages when used for specific problems.

3.2. Methods that use the Full-Wave Equations

Among methods which solve full-wave equations, finite difference and finite element methods (FEM) are most commonly employed. Both solve discretized forms of continuous equations on a grid or mesh. In the case of finite difference, partial derivatives are approximated by differences between the value of a function on adjacent grid cells. For finite element methods, a function is prescribed to each grid cell (finite element) and solved locally. In both cases, there are two options: solving the equations in the time or frequency domain. When applied to optics,

finite difference methods solve a discretized form of Maxwell's and constitutive equations in the time (FDTD) or frequency (finite difference frequency domain, FDFD) domains. Finite element methods use a different discretization of the same equations to find solutions either in the time (FETD) or frequency domains (FEFD). The perspective (Sankaran, 2019) provides an excellent overview of finite difference and finite element techniques as well as a rich set of references with more specific technical details.

Due to the nature of the algorithm, finite element methods typically allow for more flexibility in the shape of the grid elements compared to finite difference methods such as FDTD. For example, finite element methods commonly use a triangulated grid and even curved grid cells while finite difference methods typically employ a rectangular mesh. Non-rectangular and variably-sized grid cells can more accurately represent a structure, whereas rectangular cells give rise to staircasing (Akyurtlu et al., 1999; Beggs and Luebbers, 1993; Häggblad and Runborg, 2014; Liu et al., 2012; Mohammadi et al., 2005; Tornberg and Engquist, 2008); for example, a circle will appear jagged and is progressively better-represented with smaller and smaller grid cells, which adds to the computational time. While finite element methods are more efficient with non-rectangular grids, new advances in finite difference simulations have been developed that take advantage of non-rectangular mesh cells (e.g., the discontinuous Galerkin time domain (DGTD) method (J. Chen and Liu, 2013)) and other approaches (see Section 4.3 for a detailed discussion of meshing). The finite element time domain method, mentioned above, is, in fact, a combination of the finite element and finite difference methods, using the first to approximate spatial derivatives and the second to approximate time derivatives. Compared to FDTD, FETD better represents complex structures, but due to the smaller mesh sizes employed, can require a longer overall simulation time (Feng and Santamouris, 2019).Whether to choose finite element, finite difference, or one of the refined finite difference techniques that allows for more complex meshing is driven by a balance between the level of accuracy required in the representation of structures and the resulting computational time.

Another consideration when choosing between finite element and finite difference methods is whether the user's question is more naturally or efficiently answered in the time or frequency domain. Due to the mathematics of the methods and corresponding computer processing, finite element methods are more often applied in the frequency domain, where they are faster and more accurate by orders of magnitude for single-wavelength and narrowband simulations (Sankaran, 2019). In contrast, finite difference is typically applied in the time domain and is much more efficient for broadband simulations and for simulating how the electromagnetic waves evolve over time, from the source through interaction with the objects of interest and beyond.

3.3. *Efficient Methods for Specific Geometries, such as Multilayers and Photonic Crystals*

Sometimes the specific geometrical features of the structures of interest allow researchers to use more efficient simulation tools that are specifically optimized for those features. A simple and commonly used example is the transfer matrix method (TMM). It is employed to determine the reflection and transmission through multilayer structures, which are commonly seen in biology (Vukusic and Sambles, 2003) and bio-inspired structures (Kolle et al., 2013). This method works by applying Fresnel's equations to obtain the reflection and transmission at the boundary between adjacent layers, with interference effects naturally captured in the mathematics (Pedrotti et al., 2017). Transfer matrix method algorithms can be written in a variety of software programs such as the commercial *Matlab* and open-source *Python*, and already-written code is readily available on the internet.

Rigorous coupled wave analysis (RCWA) is a fast and highly efficient algorithm for more complex multilayers with lateral periodic variations across a layer. It entails writing the electromagnetic field as a sum of functions known as Bloch waves or Floquet functions, which capture the periodicity of the structures (Liu and Fan, 2012). Rigorous coupled wave analysis has been applied to biological and bio-inspired optical studies, typically in conjunction with FDTD either to validate the RCWA approach or to model non-multilayer aspects (Chen et al., 2015; Gao et al., 2011; Kim et al., 2016; Regan et al., 2016; Zhou et al., 2014). Photonic crystals, structures with periodically patterned refractive index on the length scale of the wavelengths of light being studied, can be examined through software optimized for their analysis. *Lumerical FDTD* has built-in algorithms specifically for structures of this type. The free software *MIT Photonic Bands (MPB)* is optimized to calculate the band-structure of photonic crystals, which provides information about which wavelengths of light can pass through the structures and which would be reflected at specific angles (Johnson and Joannopoulos, 2001), as is seen in many iridescent organisms (Poladian et al., 2009).

If the light is known to travel mostly along a single direction (like in an optical fiber) and the refractive index contrasts are small, one option to save computational time is to use the slowly varying envelope approximation (SVEA), also known as the paraxial equations, which allows users to significantly increase the mesh size and thus reduce computational time. The slowly varying envelope approximations can be used only for narrowband (not broadband) sources and provide the underlying mathematics for simulation tools such as the beam propagation method (BPM) (Saijonmaa and Yevick, 1983; Huang and Xu, 1993). Beam propagation has been applied, for example, to determine that the initially-proposed graded index model was insufficient to explain light propagation in the eyes of many butterflies, and that absorption is also important (Kim, 2014) A significantly more accurate method compared to the slowly varying amplitude approximation is the eigenmode expansion (EME) method, which solves for the modes (characteristic electromagnetic field distribution) given a cross-section of a fiber or multilayer without making the assumptions inherent in SVEA (e.g., EME is appropriate if refractive index contrasts are high, or a broadband source is simulated; see Gallagher and Felici (2003) for discussion). This method is more computationally expensive than SVEA but significantly more efficient than FDTD when simulating propagation over long distances. To our knowledge, the eigenmode expansion method has not been applied to biological structures, but may be useful for researchers to consider.

Highly disordered or quasi-ordered structures can and have been modeled by FDTD (Davis et al., 2020b), as described in Section 2, but can also be more efficiently modeled by Monte Carlo methods (Hwang et al., 2021). The key aspects for light interactions in these structures are multiple scattering, in which the direction of light travel and its polarization are randomized, and interference of the scattered waves. Monte Carlo is a broad class of numerical approaches which involve drawing from probability distribution functions at each computational step. In optics, Monte Carlo simulations typically involve launching photon packets in a medium, and simulating each scattering event by assigning new direction, phase, and polarization to the photon packet from physically relevant probabilistic functions. The method is implemented in many optical subdisciplines, including the fundamental biological optics of features for which multiple scattering is a major determinant of color. For example, Monte Carlo methods would be useful to study the 3D spongy β-keratin nanostructures in bird feather barbules that produce angle-independent blue and green structural color (Saranathan et al., 2012), the bird-inspired lab-based analogues (Gonome et al., 2020; Hwang et al., 2021), the prediction of light propagation through tissues for medical applications (Zhu and Liu, 2013) and atmospheric studies of light scattering in clouds (Plass and Kattawar, 1967).

3.4. *Methods that Capture Molecular, Atomic, and Quantum-Mechanical Effects*

Thus far, the simulation techniques described have employed coarse-grained models of materials, where phenomena such as refraction (light

bending) and absorption are simulated through bulk material properties such as the complex refractive index (see Section 4.2), rather than a detailed picture of the processes occurring at the atomic scale. Researchers who wish to study those types of optical phenomena and others not captured in detail by FDTD, such as fluorescence (e.g., of siphonophore lures (Haddock et al., 2005)), and shape-changes of molecules upon light absorption (e.g., retinal isomerization in the eye (Mata et al., 2002)), require other classes of simulation techniques. Density functional theory (DFT) is a method of simulating quantum mechanical effects to obtain the energy levels of molecules or systems of molecules, from which the absorption spectra can be determined (Capelle, 2006). Molecular dynamics simulations are more coarse-grained than density functional theory and give information regarding the configuration and motion of molecules and can be applied to determine the nature of light energy dissipation post absorption, for example through the excitation of molecular vibrations and other configurational changes (Hansson et al., 2002; Karplus and Petsko, 1990; Wildman et al., 2016). Researchers often combine the two tools, using molecular dynamics simulations to calculate the molecular arrangement of the system being studied at a particular moment or when exposed to a particular environment or set of stressors, and then applying density functional theory to that configuration to determine the electronic structure of the system— and subsequently the absorption of light (Wildman et al., 2016). FDTD, FEM, geometrical optics, and other techniques mentioned in Section 3.1-3.3, are not capable of capturing such fundamental quantum processes and molecular motions, and therefore would not be applicable if those are the types of light-dependent processes of interest.

4. A Primer on FDTD

At the most basic level, FDTD software simulates the interaction of light with a structure within a medium. The user can define and modify all parameters in the simulation, including features of the light source, structure(s), and medium. FDTD is useful for researchers who wish to (i) study nano and microscale architectures from simple multilayers to more intricate, convoluted structures; (ii) simulate a naturalistic, broadband light source (rather than single wavelengths at a time); (iii) vary parameters (such as structure size, shape, or refractive index); and (iv) test potential bio-inspired applications prior to their fabrication.

The way light propagates through a medium and interacts with materials, neglecting quantum effects, can be mathematically described by (i) a series of coupled partial differential equations known as Maxwell's equations together with (ii) constitutive relations that connect the presence of the field to the response of the material (e.g., the polarizability, how much the electrons can be displaced by an electric field). FDTD solves a discretized form of these equations over a grid or mesh in discrete time steps in order to determine the behavior of electromagnetic fields over space and time as they encounter various objects defined by the user or travel unhindered through the medium. The simulation proceeds until the default (1000 fs in *Lumerical*) or user-defined simulation time elapses, or the simulation can end earlier if the fraction of electromagnetic energy remaining in the simulation relative to the initial source falls below a default (10^{-5} in *Lumerical*) or user-specified *auto-shutoff* level.

When the travelling light encounters an interface between materials with different physical properties (the complex refractive index, discussed in detail in Section 4.2), it can be reflected, refracted (bent), absorbed, diffracted, and/or scattered. Researchers use the outputs of FDTD simulations to quantify and visualize these effects. In biological and bio-inspired optics, FDTD is used to quantify reflectance and transmission as a function of viewing angle and wavelength, calculate scattering cross-sections and the power distribution of light scattered in different directions, determine the profile of the light in the near field and calculate it in the far field, obtain the diffraction orders of a grating and their relative intensity, determine the photonic band structure of a photonic crystal, and much more (see examples in Section 2).

A software program commonly used for FDTD simulations of biological structures is *Lumerical FDTD*, which will be the focus of the discussion here. *Lumerical* provides a convenient graphical user interface with built-in objects (e.g. cylinders, spheres, pyramids, diffraction gratings of specific types, etc.); light sources that emit a pulse of light when the simulation starts; and monitors that store light's electric and magnetic field at specified locations, viewing angles, wavelengths, and times. Other built-in objects include boundary conditions, which define what happens to the light at the edges of the simulation domain, and analysis tools (e.g., band structure calculations, far field projections, and more). Each of these objects has a suite of settings that can be specified in their respective settings window, such as their x, y, z coordinates, material properties, and more specialized settings. *Lumerical* also provides several scripting interfaces: a global interface, for which a separate script file can be written that affects the entire simulation, as well as local interfaces, allowing users to individually modify the script describing an object in the settings tab (rather than manually entering the information). Scripting streamlines many processes, such as testing options for shapes and refractive indices or running parameter sweeps. The script language is straightforward to learn, is well-documented, and can be used alone or in combination with the graphical interface.

While *Lumerical* requires a license, a popular open-source FDTD solver is the *Massachusetts Institute of Technology Electromagnetic Equation Propagation* (*MEEP*) simulation tool (England et al., 2014; Kolle et al., 2013; McDonald et al., 2020; Oskooi et al., 2010). In general, the workflow and decision points are similar to *Lumerical*, but there is no graphical user interface; rather, everything is fully scriptable in *Python*, *C++*, or *Scheme*. The main differences between *MEEP* and *Lumerical* are the ways in which various objects are specified and which features are built-in versus what must be written from scratch by a user. For example, *Lumerical*, unlike *MEEP*, conveniently provides an automeshing feature, which assigns a non-uniform mesh with grid sizes determined by the objects in the simulation domain. The automeshing algorithm is designed to minimize numerical errors that may arise due to dispersion (errors that accrue when a computer solves continuous equations, like Maxwell's equations, in discretized form). Thus, it is critical for a user to ensure that the simulation is numerically stable in *MEEP*, while this is less of an issue in *Lumerical*. A benefit of *MEEP* is that experienced programmers can choose to fully customize the solver source code to maximize efficiency for their particular application. For example, by taking advantage of global variables, researchers can use a single script to perform parameter sweeps with nonlinear step values (as might be the case when sweeping over large length scales). Excellent references to learn more about *MEEP* are (Oskooi et al., 2010) and online documentation provided on the *MEEP* website. There are other commercial and open-source FDTD solvers not mentioned in this primer, but readily found online, that a reader may wish to consider. Finally, it is worth noting that experienced researchers can write their own FDTD script using *MatLab* or other programming platforms (Rao, 2016), though this can be quite an involved task (as all aspects — including light source, boundary conditions, objects, and mesh — must be properly coded, and careful tests should be employed to identify any unphysical behavior due to numerical or coding errors).

A simulation can be run on any one of the following platforms, with — typically — progressively faster runtime: 1) one or more cores of a local computer (a typical laptop or desktop); 2) a more powerful, remotely-accessed computer; 3) multiple machines on a local network; or 4) a computer cluster or cloud platform (3 and 4 are both examples of distributed computing). Conveniently, FDTD does not always require high performance computing: in many cases, a typical laptop or desktop can complete a simulation within a few hours. For example, in Davis et al. (2020), each simulation of an array of melanosomes spanning 5 μm in super black fish took about 45 minutes on a laptop with 8 cores and 64 GB of RAM. An 8-core computer (Intel® Xeon® Processor E5-2687W) with 64 Gb of RAM installed was used to run the simulations in

McCoy et al. (2019). The duration of simulations for the smallest lenses (~10 nm across, 5 mesh cells/nm) was several seconds, while the largest ones (~10 μm across, 14 mesh cells/ micron), required ~2 hours on the same computer. In McCoy et al. (2021), the 15-point manual parameter sweep over barbule angles in red bird feathers took about 6 hours on a laptop with 6 cores and 16 GB of RAM. Parameter sweeps and optimizations entail multiple similar simulations running in sequence or in parallel, which commonly are run using multiple computers. Section 4.7 provides a brief discussion of assessing and adjusting memory requirements.

4.1. Gather and input structural information

Researchers can either directly input experimental data or draw idealized forms based on experimentally-observed structures. The first option has the advantage of representing complicated structures, while the second can mitigate experimental artifacts and streamlines certain aspects of the modeling such as parameter sweeps.

4.1.1. Decide whether to perform 2D or 3D simulations

For any simulation, it is important to first decide whether to perform a 2D or 3D simulation. As our world is three dimensional, a 3D simulation is naturally ideal. However, the computational time is significantly higher with a higher number of dimensions, motivating 2D simulations if appropriate. Structures which are long and uniform in the out-of-plane direction (resembling a shape extruded into and out of the page) are particularly amenable to 2D analysis. Some examples include guanine platelets stacked upon one another (Rosenthal et al., 2017), bird feathers with repeated barbule structures (McCoy et al., 2021), cylindrical melanosomes in bird feathers (Nordén et al., 2021), or the effect of organelles on scattering from single cells (Dunn et al., 1997). 2D simulations reduce the time and computer memory requirements in the simulation of large structures with feature sizes over several wavelengths, such as those that are rotationally symmetric. Fig. 3 shows an example of 2D (Fig. 3A-C) and 3D (Fig. 3D-F) simulations in biological optics. In *Lumerical*, the user selects the dimension of the simulation in the *General* tab, where the refractive index of the background medium, simulation time, and temperature are also specified.

4.1.2. Gather experimental data

In order to obtain experimental data on the structure of interest, researchers use four main techniques: scanning electron microscopy (SEM), focused ion beam (FIB) imaging (sometimes in combination with SEM), transmission electron microscopy (TEM), and computerized tomography (CT).

SEM is typically employed to image the surface of a sample and has been used for optical analyses of many biological features, from feathers and beetle cuticle to fish scales (Gorb, 2009; Vukusic and Stavenga, 2009). The interior can also be observed, for example by slicing the sample open with a razor blade or freeze fracturing. SEM can attain a resolution of ~2-10 nm depending on the instrument (Vukusic and Stavenga, 2009) as well as the sample characteristics and preparation method (e.g., resolution is lost with excess charge buildup in samples consisting of non-conducting materials, which can be mitigated through metal coatings).

FIB builds up a 3D image of a biological material by using focused beams of ions to alternate between slicing the sample and viewing the newly exposed surface (Milani et al., 2007). Alternating between slicing and imaging modalities is achieved by varying the conditions of the ion beam (Milani et al., 2007) and software is employed to reconstruct a 3D image. The best resolution currently achievable with FIB imaging is ~1 nm (Fibics Incorporated, 2021). A FIB instrument can also be equipped with an SEM (FIB/SEM) to generate 3D images as ion bombardment by FIB is employed to shave away layers of the sample and the newly exposed surfaces are imaged by SEM (Galusha et al., 2008; Smentkowski et al., 2006; Vukusic and Stavenga, 2009; Wilts et al., 2018b; Yun et al., 2018). FIB/SEM results in beautiful 3D images with the same lateral resolution as SEM (Fig. 3E; (Wilts et al., 2018b)) but, like FIB alone, tends to be time and resource intensive as alternating slicing and imaging is a slow process.

TEM is one of the most commonly employed methods for observing the interior of the sample, reaching 2-10 nm resolution, though it typically significantly outperforms SEM in terms of resolution due to the thin size of the sample, leading to a lower excitation volume and reduced electron scattering within the bulk of the material. However, sample preparation is substantially more complicated than for the other techniques, typically requiring embedding the sample in a resin and cutting it into < 100 nm slices (Vukusic and Stavenga 2009). TEM has been used to examine structures responsible for optical effects in skin (e.g., arrangement of collagen, iridophores, and chromatophores (Rosenthal et al., 2017; Davis et al., 2020b), algae cuticle (Chandler et al., 2015), and bird feathers — particularly structural colors from melanosomes within feathers (Eliason et al., 2013) — among many others).

Biological samples studied with SEM typically need to be coated in gold or another conducting material to prevent the build-up of electron charges on the sample surface that deflect the incoming beam of electrons, thus distorting the image. High vacuum operation is needed to prevent electron scattering before reaching the sample. Imaging samples in such an environment requires them to be dry (e.g., through critical point or hexamethyldisilazane (HMDS) drying), though this creates potential size or shape distortions in biological specimens (see Bagge et al., 2016 for examples of how to compensate for these changes). Environmental SEMs (ESEMs) can be used to image wet samples, as they operate across a wider range of conditions, though the resolution tends to be lower (but can reach as fine-grained as ~5 nm, (Wang and Lee, 2008)).

Computerized tomography (CT) is an excellent alternative for the observation of samples in 3D as it does not require excessive preparation (typically, the only sample preparation step for CT is staining with iodine (du Plessis et al., 2017)); a disadvantage, however, is that the resolution is lower than for the electron microscopy technique, as the smallest feature that can be distinguished through standard CT is ~100 nm. CT produces 3D scans of an entire sample (interior and exterior), by collecting a "stack" of 2D X-ray images of the sample; software is then used to process the stack into a 3D structure. With nano-CT or micro-CT, pixel size ranges from ~500 nm to 150 μm (du du Plessis et al., 2017) but can, in specialized instruments, reach as low as 50 nm (Sasov et al., 2011). Besides its relatively lower resolution, a major challenge of CT is preventing sample movement, because the scanning typically involves rotating the sample.

Another common characterization technique is synchrotron small angle X-ray scattering (SAXS), a method with an impressive resolution of roughly 10 Å, often used to assess the long- and short-range order of biological structures (Saranathan et al., 2012; Skou et al., 2014). Further, evermore sophisticated optical imaging techniques and algorithms are being developed with increasingly better resolution and options for imaging through 3D materials (Verstraete et al., 2019). Which tools (or combination of tools) are used largely depends on the instruments and expertise available in a lab and the resolution required to observe specific structures of interest.

4.1.3. Input data into the FDTD simulation

Experimental data is precise but finicky; microscopy and tomography at small scales can produce gaps or artifacts in the image which need to be processed before simulation. Microscope images or 3D scans of structures can be imported and fine-tuned via the *Lumerical* import wizard. For example, microscope images can be imported as PNGs or JPGs, and refractive indices can be assigned to different components of the resulting grayscale image (Fig. 3C). The image can be extruded in the Z direction for a defined length. For an example analyzing TEM images see (Chandler et al., 2015; Wilts et al., 2014) as well as Fig. 3.

Often, researchers draw idealized forms based on the data they

observe and measure. Such idealized structures may not be exact, but they allow for parameter sweeps and can offer greater interpretability. In fact, drawing one's own structures gives the user the opportunity to sequentially build up complexity: what is the simplest geometry that can explain the observed optical properties, and what is the role of each of the components discovered experimentally? A user can draw structures in *Lumerical* through the scripting and/or graphical user interfaces, or by using another scripting or computer aided design (CAD) software and importing the image. *Lumerical*'s object library includes structures such as spheres, cylinders, and various polyhedra. To create specific geometries that are not included in the scripting library, researchers can write code to modify existing functions. For example, the sphere function can be modified to make ellipsoids with a specified aspect ratio/size (Davis et al., 2020b), and custom shapes can be drawn using equations in the script (McCoy et al., 2019). Figs. 4 and 5 show examples of a typical workflow, wherein the image from microscopy is recreated to the best approximation. In Fig. 4, a large array of randomly placed ellipsoids represent their real counterpart, discovered in the skin of a super-black fish. In Fig. 5, a single micro-bump of a peacock spider is produced through plotting a custom superellipsoid equation including radius, height, and shape.

4.2. Determine and assign refractive indices of the material and surroundings

Once a structure is input or drawn into the simulation domain, its material composition needs to be assigned. Optically, materials are characterized by their refractive index $\underline{n}$, a complex number, whose real part n quantifies the apparent reduction in the velocity of light as it passes through a relatively more polarizable material compared to its speed in vacuum, $c = 3^{*}10\hat{}8$ m/s; and imaginary component k quantifies light attenuation in the material due to absorption:

$$\underline{n} = n + ik$$

When light moves encounters a boundary between materials with different refractive indices — such as between air ($n = 1$) and a bird feather where the exterior is composed of keratin ($n \sim 1.53$ (Leertouwer et al., 2011)) — some fraction is reflected and the rest bends, or refracts; if the feature sizes of the materials are close to the wavelength scale of light, scattering will be observed. The attenuation coefficient k can vary by orders of magnitude, contributing to the opacity of the material. Materials like melanin have a a high attenuation coefficient ($k \approx 0.076$ for light with 540 nm wavelength (Stavenga et al., 2015)) while unpigmented butterfly chitin has a negligible value of k for all visible wavelengths (Leertouwer et al., 2011) and can be set to 0 for most simulations. Likewise, materials can differ in their dispersion, i.e., how strongly both the real and imaginary parts of the complex refractive index vary with wavelength. Melanin has high dispersion (Stavenga et al., 2012) while that of chitin is quite low over the visible wavelength range (Stavenga et al., 2016).

Lumerical has an extensive library of built-in materials with wavelength-dependent real and imaginary components of the refractive index, but most of them are not useful for biologists (e.g., gold, platinum, and silicon). *Lumerical* allows users to add custom materials not included in the standard library. A text file is needed to create a new material; it contains three columns: wavelength (in nm), n (the real part of the refractive index), and k (the imaginary part of the refractive index). Once this data is imported into the database, it will be fit with one of several generalized multi-coefficient models. Common equations used to fit the refractive index as a function of wavelength include the Cauchy equation, a good approximation for transparent materials in certain wavelength regimes; the Sellemier equation, applicable to transparent materials for a broader range of wavelengths; and various oscillator equations such as the Lorentz oscillator model for absorbing materials. The accuracy of the fit can be improved by adjusting fit parameters. An important characteristic of the equations is that they satisfy the Kramers-Kronig relations (Kinsler, 2011), mathematical expressions relating the real and imaginary parts of a complex function (such as the refractive index) to one another and which are a direct consequence of causality (effects cannot precede their cause) in physical processes. The necessity to satisfy Kramers-Kronig has two practical consequences. First, it is a good checkpoint as to the validity of a model: if the obtained real and imaginary parts of the refractive index do not satisfy Kramers-Kronig, then the experimental measurement and/or fit are erroneous and should be reassessed. Second, it can simplify measurements: one only has to measure either the real refractive index or the absorption as a function of wavelength and can obtain the other by plugging into the equation. The Cauchy equation should thus be used with caution as it does not satisfy Kramers-Kronig, and therefore is unphysical; it is, however, a simple approximation that gives reliable results for certain wavelength regimes and types of materials; the other mentioned equations do satisfy Kramers-Kronig.

Obtaining the true refractive index of biological materials is typically challenging and is often a main bottleneck in performing trustworthy optical modeling (Vukusic and Stavenga, 2009). Practically, values for the refractive index as a function of wavelength of biological materials can often be found in the literature (though care must be taken to ensure that the experimental method used was valid and that the material is comparable to the one under investigation; for example, refractive index changes if a material is packed differently on the molecular level and thus has higher or lower density, or if it contains more absorbing material such as pigments, which would raise both the real and imaginary parts of the refractive index). Alternatively, the refractive index can be obtained by applying the Kramers-Kronig equation to absorption data, as briefly mentioned above. Absorption is often simpler to obtain experimentally; a common strategy involves refractive index matching (infiltrating the material with a liquid of approximately identical refractive index and negligible absorption) to remove scattering at boundaries between material and air. The percent light transmitted through the infiltrated material is then measured and converted to absorption through the Beer-Lambert law. This approach has been applied to many biological samples, including fly photoreceptors (Stavenga and van Barneveld, 1975) and butterfly wings (Wilts et al., 2017).

To attain the refractive index directly, scientists often use refractive index matching, wherein liquids of varying composition are infiltrated into the biological structures until any structural color is eliminated, indicating loss of index contrast between the liquid and the biological material (Mason, 1927). This technique is well-suited to structures with no refractive index variation across the sample, or refractive index variations on length scales well below the wavelengths of light of interest, allowing for an effective refractive index to be used. This method is not the most accurate as preparing solutions with precise refractive indices is not straightforward. Recent work demonstrated a new method to tune the refractive index of water-based solutions based on the Kramers-Kronig relationship, by using commercially-available dyes (Sai et al. 2020); this approach was extended to polymers through the incorporation of plant-based pigments with specific absorption spectra (Yasir et al., 2021).

Jamin-Lebedeff (also spelled Jamin-Lebedev) interference microscopy is one of the most sensitive techniques employed to obtain the refractive index of a biological material. Basic Jamin-Lebedeff interference microscopy works as follows (Jamin, 1868; Lebedeff, 1930; Stavenga and Wilts, 2019): an incident light beam is split by a crystal into two spatially separate, perpendicularly polarized beams that pass through (i) the test object and (ii) an object (typically a liquid) of known refractive index. The beams are recombined by a second crystal, and the phase shift in the test object reveals the refractive index. Although this method was classically used for transparent material (Gillis and Wibo, 1971), it can be used for pigmented tissues as well as was demonstrated in a study of red-winged damselflies *Hetaerina americana* (Stavenga et al., 2013). Ellipsometry is a more standard materials characterization

technique providing accurate measurements of the refractive index and is particularly useful for well-defined, smooth thin films, such as those of the multilayer polymer fibers inspired by the seed coating of the *Margaritaria nobilis* fruit (Kolle et al., 2013).

The refractive index of a material can also be modelled. For example, researchers often apply effective medium theories to determine an effective refractive index for composite materials where material variations occur on length scales much smaller than the wavelengths of light being studied (~λ/10 or below). The refractive index is essentially given as the sum of the refractive indices of each material weighted by its relative volume fraction, both of which may be known through other measurements described above (Bagge et al., 2016; Freyer et al., 2019; Hwang et al., 2021; Stavenga et al., 2017; Zhang et al., 2020). If refractive indices are unknown, various more fine-grained models, which account for the motion of electrons, can be applied, include the Drude and Lorentz models, which treat electrons as free (as in a metal) or bound by a spring force, respectively (Ashcroft et al., 2016), or density functional theory and/or molecular dynamics simulations can be applied to predict the refractive index (Lee et al., 2012; Park et al., 2011).

Once the refractive index is known to a satisfactory degree and input into *Lumerical*'s material database, the materials can be assigned to the structures created as described in 3.2. A refractive index should also be assigned to the background medium (e.g., n = 1 for air and n ~ 1.334 for water for the 400-700 nm wavelength range). An advantage of computer simulations is that for the plethora of cases where the refractive index is not known, parameter sweeps can be performed around an estimated value.

4.3. Set the mesh size

Meshing is a balance between speed and accuracy as small differences in mesh size can have large impacts on simulation time: coarse mesh sizes run more quickly, but are likely less accurate. Simulation time is proportional to *(1/dx)^4* and *(1/dx)^3* for 3D and 2D simulations, respectively, where *dx* is the length of a mesh cell, as described in *Lumerical*'s documentation on meshing considerations; the memory requirements scale as *(1/dx)^3* and *(1/dx)^2*. The mesh should be small enough to well-represent the light and all objects in the simulation; thus, a typical recommendation is to set the mesh grid size to fit ~8 boxes per wavelength in the material with highest refractive index. That is, the length of each grid is recommended to be *(1/8)* lambda_min/ n_max*, where *lambda_min* is the smallest wavelength of interest as measured in vacuum and *n_max* is the highest refractive index in the structure or medium (Oskooi et al., 2010). The simulations are then run with finer and finer mesh sizes until the output of the simulation converges. The recommendation is to choose the *auto non-uniform* mesh option in *Lumerical*, which is a built-in automeshing tool that creates a non-uniform mesh, with a finer mesh where necessary (in locations with higher refractive index, with smaller feature sizes, and at material interfaces) and a coarse mesh where possible to save memory and time (such as regions of the object without small-scale features) while preserving numerical stability.

A user can choose an accuracy level in the range 1-8 in the automeshing settings, where 1 is the lowest accuracy and corresponds to 6 points per wavelength and each subsequent value is 4 points per wavelength higher than the previous (i.e., increasing the accuracy from 1 to 2 to 3 corresponds to moving from 6 to 10 to 14 points per wavelength). It is useful to start with the lowest accuracy of 1 when testing simulation setup. Once the simulation setup has been verified, *Lumerical* recommends accuracy levels between 2-5 for most applications, as determined through convergence tests. *Mesh override regions* are also available in *Lumerical* (selected in the graphical user interface) to indicate locations with a different mesh resolution than the overall simulation. It is particularly useful to place such regions over particularly small features of objects and along interfaces between two materials, and to define a smaller mesh in these regions compared to the rest of the simulation.

Traditionally the mesh for FDTD has been made up of regularly tiled rectangles (for 2D simulations) or rectangular prisms (for 3D). However, over the past 20 years, new forms of meshing have been developed that aim for similar object fidelity as with finite element methods, but with the benefits (such as broadband sources) of FDTD methods. *Lumerical* offers some of these new options in its software, which can be selected under the "*mesh refinement options*" tab. The methods include the standard *staircasing*, in which case the mesh cells and Yee cell are identical; several *conformal variant* methods, which apply Maxwell's integral formalism at material boundaries, increasing the accuracy of the representation of the geometry while maintaining a similar or better efficiency than offered by a rectangular grid (Yu and Mittra, 2001); *dielectric volume average* method, which is useful for interfaces between materials with very small refractive index difference; and others for more specialized situations (see *Lumerical* documentation and detailed discussion in (Gedney, 2011; Taflove, 2007; Taflove et al., 2005). The general recommendation is to use the *Conformal Variant 0* method for most simulations, except those involving metals (e.g., in a bio-inspired application), in which case *Conformal Variant 1* should be used.

4.4. Define a light source

Light varies in its electromagnetic field distribution, spectrum, angle of incidence, and polarization. *Lumerical* provides 5 choices of light sources to add to the simulation: *plane wave*, *Gaussian*, *dipole*, *total-field scattered-field (TFSF)*, and *mode source*. It is also possible to import a custom light source with a user-specified electromagnetic field profile at the source injection plane and the script *setsourcesignal* function allows a user to customize the time signal of the source. In all cases, the user specifies the source type, its spectrum, polarization, location, pulse duration, and — if relevant — the propagation direction and relative phase in the case of multiple sources.

The choice of source type depends on the question of interest, as some source types might be more accurate than others at representing the actual light source used in experiments. For example, a plane wave source of the *periodic/Bloch* type is used to inject a uniform electromagnetic field along an infinite line (in 2D simulations) or plane (in 3D simulations) traveling in a user-specified direction. It is the appropriate choice when the structure is very large ($\gtrapprox$ 10 wavelengths across) and is illuminated by a light source which is far enough away that the spherical waves emanating from the source are significantly larger than the object and can be therefore be approximated as plane waves over the extent of the object. Plane wave sources are typically used in conjunction with periodic boundary conditions, in which case the extent of the object and the plane wave are both infinite; this is common for simulations involving biological materials which can be modeled as a repeating unit cell or representative volume element (Chandler et al., 2015; Davis et al., 2020; Jacobs et al., 2016). A user would select plane waves of the broadband fixed angle source technique (*BFAST*) type if the simulation involves non-orthogonal injection of a plane wave together with periodic boundary conditions. A third option is *diffracting*, in which case the plane wave passes through a slit (aperture); to our knowledge, this option is less commonly employed in biological and bio-inspired research.

The infinite plane wave source does not provide valid results when the structure size is only a few wavelengths across because diffraction and interference effects at the edges will dominate. Researchers often use Gaussian sources as an alternative source when at least one of the assumptions required for plane waves breaks down. The Gaussian source represents a beam with an amplitude equal to the Gaussian cross section of a given width, traveling in a user-specified direction. This source is also representative of light being focused, e.g., by a microscope objective, or when the light source has a shape that can not be approximated by a plane wave in the far field (Agez et al., 2017; Saba et al., 2014).

The total-field scattered-field source (sometimes referred to as the

Huygens surface method, total field/scattered field, or similar variations) is often employed to calculate the scattering cross-section and angular distribution of scattering objects in the simulation. It is quite useful in biological studies aimed at understanding the role of individual scatterers or collective scattering from many features, and has been applied to the microstructures within the wings of a variety of butterflies (Lee and Smith, 2009; Siddique et al., 2013; Wilts et al., 2017) as well as to bio-inspired devices, such as those involving scattering from assembled colloidal structures or scatterers or light concentrators with shapes derived from biological organisms (Narasimhan et al., 2020; Yamashita et al., 2020). The total-field scattered-field source divides the domain into two regions: (i) the source region where a finite plane wave source is injected and (ii) the scattered region, where the object is located; electromagnetic waves collected by monitors in the first region are subtracted from those in the second to obtain the scattered light only (Potter and Bérenger, 2017).

Dipole sources are used to simulate point-source radiators, with an electromagnetic field propagating in all directions. They are appropriate for simulations of small radiators in biology such as fluorescent molecules or bioluminescent bacteria (Golberg et al., 2014; Lotan et al., 2017). The remaining mode light source is, to date, less commonly used by natural scientists, but can be valuable in specific situations, such as finding the guided mode of tubular multilayer reflectors (e.g., in *Galiteuthis* (Holt and Sweeney, 2016)).

In case of uncertainty about the choice of source, it is a good idea to simulate the source in free space (no objects for the light to interact with), using the same boundary conditions and mesh that would be used for the actual simulation. A movie monitor (discussed in Section 4.6) can be used to visualize the propagation of the light. Once a light source has been selected, its spectrum can be modified to better represent the illumination conditions. For example, researchers can reduce the relative contribution of red light for underwater simulations where these wavelengths do not penetrate as far as other colors, or they can model sunlight by using the script command *solar()* in *Lumerical* and assigning it to the light source. Laboratory and microscope illumination also have specific characteristics, which can likewise be modeled through changing various aspects of the light source used in the FDTD simulation.

4.5. Set simulation boundaries

FDTD simulations run over a defined region of space (the "simulation volume"). It is thus important to define what happens to the light at the boundaries (edge lines in 2D simulations or edge planes in 3D simulations). For example, it would be imprudent to have light bounce from the boundaries back into the simulation domain as it would interact with light emanating from the structures, creating simulation artifacts such as interference patterns. To avoid such effects, "perfectly matched layer" (PML) boundary conditions have been developed to minimize reflections from the boundaries through a concept prevalent in wave engineering known as impedance matching (Berenger, 1996, 1997). In the case of optics where magnetic field effects are not important, impedance matching is the imposition of a smooth transition between two media with different refractive indices. Perfectly matched layers are useful for any boundary that is beyond the interest of the study, such as the bottom edge in a study of beetle cuticular surfaces.

Another common boundary condition used in biological simulations is the periodic boundary condition. Periodic boundaries are useful either for disordered structures that extend over a large distance, such as the randomly distributed ellipsoids of the fish skin in Fig. 4 (periodic boundary conditions are used on all sides of a representative volume element except the top and bottom of the simulation in Fig. 4C), or for periodic structures, for which periodic boundary conditions are used around a single repeating unit such as in the peacock spider cuticle in Fig. 5. The use of periodic boundary conditions, rather than simulating a larger extent of the structure, saves time and computer memory.

Periodic boundary conditions require a note of caution. Although simulating a single unit of the structure is a useful strategy, it can often lead to spurious peaks or valleys in reflectance/transmittance due to resonance or interference. These results are often not seen in reflectance measurements taken from the animal because the biological surface is not perfectly periodic; there is some randomness in each unit. To avoid these spurious peaks, it is often useful to average multiple simulations of the same structure with slightly different sizes. In the example of the butterfly scale, spurious peaks can be eliminated by simulating unit cells that span 95%, 97.5%, 100%, 102.5%, and 105% of the desired structure (Davis et al., 2020a). Other aspects to pay attention to are the type of light source used and its direction of incidence (for non-perpendicular incidence, Bloch boundary conditions with the broadband fixed angle source technique should be used, as mentioned in Section 4.5). In cases where the structure of interest has a reflective backing (e.g., guanine platelets or thick layers of collagen), it may be useful to employ a metallic boundary condition instead of a PML boundary. Metallic boundaries act as perfect conductors, reflecting any incident light. While biological reflectors are not perfect, it may be a more representative choice than PML boundaries, particularly in the case of materials where small reflections from backing layers may contribute heavily to overall reflectance (for an example, see (Davis et al., 2020b)).

Finally, as a rule of thumb to prevent artifacts in simulation, users should set the size of the simulation region, monitor, and source to be large enough that there is no clipping of the fields. Also, the source should not be too close to any monitors (at least 2-3 mesh cells away). It is important to place these, and most other, boundaries at least half a wavelength away from any structure in order to avoid numerical artifacts such as light from a structure being artificially absorbed by the perfectly matched layer. In general other objects can be close together, but users should consult the *Lumerical* guidelines for their specific setup.

4.6. Add reflectance and transmission monitors to record data

Now that the biological structure, background medium, light source, and boundary conditions have been defined, it is necessary to add monitors to collect the electromagnetic field over the course of the simulation. *Lumerical* offers several options: *frequency domain field profile*, *frequency domain field and power*, *movie*, *field time*, and *mode expansion* monitors; more than one monitor can be, and often is, used in the same simulation. For example, by placing two frequency domain monitors above and below the structure users can simultaneously collect reflection and transmission data. The user can specify various options in the settings tab for each of these types of monitors (or in the script), including their position in space, the frequency components and time points at which to collect data, which type of data to collect (e.g., specific components of the electric field or the total power). These monitors contribute significantly to the simulation memory requirements, especially if they span a large area, and therefore it is recommended to only collect the data that is necessary (e.g., by reducing the number of frequencies, time points, and spatial locations). Monitors can be a point, line, box, or 3D rectangular structure.

Most often, biologists wish to understand how much light of specific wavelengths is transmitted through or reflected by a structure, as well as scattering and diffraction effects. "Frequency domain field and power" monitors are the ideal choice in this case as they provide the Fourier transform of the time-domain signal (i.e., the spectrum of the collected light). A common simulation in biological and bioinspired research is to place one such monitor above and a second one below the structure to gather reflected and transmitted light, respectively, including proportional amounts and presence of light of different colors (wavelengths). Researchers can analyze the angular distribution of the collected light to determine the diffraction orders and proportion of light scattered into each order, in the case of a grating structure, or calculate the radial distribution of scattered light around individual structures for comparison to reflectance distribution functions (England et al., 2014; Rosenthal et al., 2017). One can also place monitors inside the structure to

measure transmission through a subsection of the structure being investigated (McCoy et al., 2021). Note that there are two very similar types of frequency domain monitors, but biology researchers typically use the "field and power" monitor, which snaps to the nearest mesh cell, providing more accurate results regarding the power in the electromagnetic field.

"Field time" monitors record the electromagnetic field at specific locations in the simulation over time. This is useful for time-of-flight studies, which measure how much light scattering occurs internally before light leaves the structure (Meiers et al., 2018; Tanifuji et al., 2004). Field time monitors are also commonly used to obtain the band structure of a photonic crystal (such as the slab photonic crystals of many diatom skeletons (Goessling et al., 2020)), as randomly-oriented and dispersed dipoles emit light and the monitors capture the light over time. Modes of the photonic crystal are the longest-lived and can be identified as peaks in the Fourier-transform of the time signal. The field time monitors can also be used to check that the user-specified simulation time is long enough by checking that the electromagnetic field has been fully captured by the monitor.

"Movie" monitors record a movie of the light starting as an initial pulse emitted from the light source and then interacting with the structure (Wilts et al., 2014). They are very valuable to visualize the interaction of light with the structures under investigation. Movie monitors are the only monitor type that increases not only the simulation memory requirements, but also the simulation time.

In addition to reflectance and transmission, *Lumerical* has available monitors for refractive indices, charge, and more. The refractive index monitor allows researchers to view a cross section of the structure of interest as it is represented by the mesh in order to check the fidelity of the object after the mesh has been defined.

In all cases, data from the monitors can be studied within *Lumerical* software, including through the graphical user interface as well as using the script for data analysis (e.g., finding peaks, averaging the radiated power over a certain wavelength range, or projecting electromagnetic fields collected near an object to the far field). The color bars can also be adjusted to better view certain portions of the data; for example, when viewing a movie, a researcher may wish to increase the visibility of the fainter light remaining in the simulation at long times, which would saturate—and thus obscure — the initial pulse. Data can also be exported for processing by other software, for example as a. csv file which can be read by *Matlab*, *Python*, *R*, and other options.

4.7. Assess and improve computational requirements

In general, the computational time required for an FDTD simulation depends on two aspects, each containing a multitude of features: (i) the computer hardware (computational power, random access memory (RAM), processor speed, number of cores, etc.) and (ii) the specific way in which the software encodes all aspects of the simulation (Maxwell's equations, boundary conditions, electromagnetic field components, material properties at every grid point, etc.).

Once the simulation has been set up in *Lumerical*, it is possible to assess the memory required by clicking *Simulation Memory Requirements*. If the number is larger than the amount of RAM contained in the computer, memory will have to swap between RAM and the hard drive, significantly slowing down the simulation as the speed of simulations is limited by the memory bandwidth (the speed at which information can be transferred between RAM and CPU). Once a simulation is run, it can be further improved. The automatically-generated *.log* file provides information regarding the time allocated in each of the processes involved in running the simulation (initializing and meshing, running FDTD simulation, finalizing data and storing files). It is found in the same folder as the simulation and can be opened with a text editor. Guided by the information provided in the. *log* file, a user can adjust any aspects that reduce the corresponding times; for example, if the first process takes a long time, consider using a coarser mesh, or keeping a fine mesh over small features but increasing the mesh size in other regions. The *Resource Configuration* can also be adjusted (for example to use a larger or smaller number of cores) in order to lower the *total FDTD solver time* that appears in the *.log* file.

4.8. Conduct parameter sweeps

Under some circumstances, researchers wish to investigate the optical effect of varying the refractive index, size, shape, and other aspects of a natural structure; aspects of the light source; and/or features of the external environment. *Lumerical* allows parameter sweeps through the implementation of *for loops* in code or by using the built-in *Optimization and Sweeps* tab. Parameter sweeps are useful in many analyses, for example to determine whether evolution has achieved an optimum among all possible structural configurations (e.g., reflecting the most light with the minimum material necessary (Wilts et al., 2018b)), to interpret within-organism variation in color (e.g., magpie feathers that change from green to blue (Stavenga, Leertouwer, and Wilts 2018)), or to guide the design of bio-inspired engineered materials (e.g., optimizing thickness, depth, and size of nanoscale holes in butterfly-inspired high-efficiency absorbers (W. Wang et al., 2017)).

To run a parameter sweep, one indicates the minimum, maximum, and step value for the parameter as well as an output value chosen by the user, such as reflectance. When the user runs the sweep, a simulation at each parameter value will run independently and the output value will be recorded. Once this is complete, the user can plot the output value as a function of the parameter being swept. Heat maps are a useful tool to visualize the parameter space and overlay experimental data. This is demonstrated in Fig. 5E, where the shape of a peacock spider microbump is varied to investigate whether their size is arbitrary or serves a functional purpose. The heatmaps reveal that the size corresponding to the one seen in nature ($R0 = 1$) provides the lowest reflection simultaneously with the largest path length through the melanin layer beneath them, thus maximizing absorption.

Users can also implement a manual parameter sweep by gathering data at discrete points over a range. Manual parameter sweeps have the advantage of saving computational time. For example, LED lenses were designed and tested with four different heights of nanoscale grooves (inspired by firefly lanterns) to arrive at the optimum for maximally transmitting light (Kim et al., 2012). Additionally, damselflies (*Ischnura elegans*) change in color as they mature (see Section 2.2), and this color change was studied through FDTD simulations based on structures observed at four discrete timepoints in the damselflies' lives (Henze et al. 2019). As bird feather barbules vary in angle from low to high, reflectance decreases, which was observed experimentally and confirmed with FDTD simulations at different simulated barbule angles (McCoy et al., 2021).

4.9. Validate the optical model with measurements

As with any model, there is always a risk that the model does not correspond to reality for one reason or another (e.g., the geometry is inaccurate, the wrong boundary conditions are chosen, or numerical errors arise due to meshing or insufficient simulation time, among others). Thus, it is essential to perform simulations of test cases to increase confidence that the results are accurate and relevant to the biological organism studied. It is particularly useful if analytical results can be obtained to compare with the simulation results (Freyer et al., 2019).

The most convincing test of all is comparison to experimentally obtained data. For example, in many studies of structural color, researchers use a suite of experimental techniques such as hyperspectral imaging, spectrophotometry with a directional probe or integrating sphere, and scatterometry to validate their FDTD simulations. For example, the reflectance spectra of an iridescent bird feather can be measured with spectrophotometry, and the experimentally-obtained spectra can be compared to the simulated reflectance spectra from the FDTD model. A

good match between experiment and simulation indicates that the FDTD model accurately represents the most important parts of reality. Vukusic and Stavenga (2009) provide an excellent review of different tools for obtaining experimental data.

Because all models are idealized, in many cases qualitative trends rather than an exact quantitative match between experimental and model results can be valuable and sufficient. When validating an optical model, it is particularly important to look for sharp peaks in the model results that can result from idealized structure producing spurious resonance or interference effects not observed in experimental results. For example, in a study of *Flavobacterium* colonies, FDTD results produced five reflectance peaks, while experimental results only showed three peaks (Schertel et al., 2020). These spurious peaks may be explained by creating a representation of a 3D colony from a 2D, binarized TEM image. In similar cases, 3D idealized versions of the structure created within *Lumerical* may be preferable.

5. Conclusions

FDTD is a powerful tool to help natural scientists understand the physical basis of optical adaptations. In this primer, we have presented a simple overview of the FDTD workflow (Section 4), guidance for when to choose FDTD rather than another optical simulation technique (Section 3), and references to many papers that have used FDTD for biological purposes (Section 2). We show that FDTD is not only useful in characterizing the basis of structural color and other optical effects, but it also allows us to draw conclusions about the process of evolution and inspire new technologies of our own. Parameter sweeps in FDTD allow scientists to explore the space of theoretically possible photonic structures and determine whether and why living creatures evolved only a subset of all theoretical possibilities. FDTD simulations with and without particular structural features help researchers identify the structures most important to a particular optical phenomenon.

This primer should serve as a starting point for researchers interested in modeling optical effects in nature, but it is far from the endpoint. Since its first introduction by Yee in 1966, the FDTD method has seen much progress, and continues to do so as researchers develop newer algorithms that are more efficient than before and/or include additional physics (Taflove, 2007). Researchers should be on the lookout for new tools that might be of interest, such as expanded meshing options; more efficient boundary conditions; a larger range of light sources; the possibility to model quantum effects; and the interaction of light with other processes such as heat, chemical reactions, fluid dynamics, and more. As mentioned, *Lumerical FDTD* itself has evolved over the past 5-10 years, now allowing for non-rectangular mesh cells, additional physics such as thermal and electronic effects, and more.

The natural world teems with living creatures shining, reflecting, absorbing, and otherwise manipulating light. FDTD is a method — best used alongside other techniques, such as advanced microscopy — that can help researchers peek into, interpret, and learn from the wonders of our world.

Declaration of Competing Interest

The authors report no declarations of interest.

Acknowledgements

We are grateful to Stefan Kolle for valuable discussion and comments on the paper, as well as Dr. Nikolaj Mandsberg, Dr. Thomas Schroeder, Natalie Nicolas, and Shucong Li for their feedback. The work was supported by the Department of Defense, Army Research Office under award W911NF-17-1-0351. ALD and DEM conducted this research with Government support under and awarded by DoD, Army Research Office, National Defense Science and Engineering Graduate (NDSEG) Fellowship, 32 CFR 168a. This material is based upon work supported by the NSF Postdoctoral Research Fellowships in Biology Program under Grant No. 2109465 to DEM. DEM is also supported by the Theodore H. Ashford Graduate Fellowship in the Sciences and the Stanford Science Fellowship.

References

Agez, Gonzague, Bayon, Chloé, Mitov, Michel, 2017. Multiwavelength Micromirrors in the Cuticle of Scarab Beetle Chrysina Gloriosa. Acta Biomater. 48 (January), 357–367.

Aizenberg, Joanna, Sundar, Vikram C., Yablon, Andrew D., Weaver, James C., Chen, Gang, 2004. Biological Glass Fibers: Correlation between Optical and Structural Properties. Proc. Natl. Acad. Sci. U. S. A. 101 (10), 3358–3363.

Aizenberg, J., Tkachenko, A., Weiner, S., Addadi, L., Hendler, G., 2001. Calcitic Microlenses as Part of the Photoreceptor System in Brittlestars. Nature 412 (6849), 819–822.

Akyurtlu, A., Werner, D.H., Veremey, V., Steich, D.J., Aydin, K., 1999. Staircasing Errors in FDTD at an Air-Dielectric Interface. IEEE Microwave Guided Wave Lett. 9 (11), 444–446.

Ashcroft, Neil W., Ashcroft, Mermin, Wei, Dan, David Mermin, N., 2016. Solid State Physics: Revised Edition. CENGAGE Learning Asia.

Bagge, Laura E., Kinsey, Stephen T., Gladman, Justin, Johnsen, Sönke, 2017. Transparent Anemone Shrimp Become Opaque after Exercise and Physiological Stress in Correlation with Increased Hemolymph Perfusion. J. Exp. Biol. 220 (Pt 22), 4225–4233.

Bagge, Laura E., Osborn, Karen J., Johnsen, Sönke, 2016. Nanostructures and Monolayers of Spheres Reduce Surface Reflections in Hyperiid Amphipods. Curr. Biol.: CB 26 (22), 3071–3076.

Bay, Annick, Cloetens, Peter, Suhonen, Heikki, Vigneron, Jean Pol, 2013. Improved Light Extraction in the Bioluminescent Lantern of a Photuris Firefly (Lampyridae). Optics Express 21 (1), 764–780.

Beggs, J.H., Luebbers, R.J., 1993. Numerical Analysis of Staircasing Effects on Cutoff Frequencies for FDTD Modeling of Circular Waveguides. Proceedings of IEEE Antennas and Propagation Society International Symposium. https://doi.org/10.1109/aps.1993.385287.

Berenger, J.-P., 1996. Perfectly Matched Layer for the FDTD Solution of Wave-Structure Interaction Problems. IEEE Trans. Antennas Propag. https://doi.org/10.1109/8.477535.

Berenger, J.-P., 1997. Improved PML for the FDTD Solution of Wave-Structure Interaction Problems. IEEE Trans. Antennas Propag. 45 (3), 466–473.

Bermúdez-Ureña, Esteban, Kilchoer, Cédric, Lord, Nathan P., Steiner, Ullrich, Wilts, Bodo D., 2020. Structural Diversity with Varying Disorder Enables the Multicolored Display in the Longhorn Beetle Sulawesiella Rafaelae. iScience 23 (7), 101339.

Burger, S., Köhle, R., Zschiedrich, L., 2005. Benchmark of FEM, Waveguide, and FDTD Algorithms for Rigorous Mask Simulation. 25th Annual BACUS. In: https://www.spiedigitallibrary.org/conference-proceedings-of-spie/5992/599216/Benchmark-of-FEM-waveguide-and-FDTD-algorithms-for-rigorous-mask/10.1117/12.631696.short?casa_token=-V9gFmCMff4AAAAA:NpLL2WYj7dQK4eTz60latWoXe67x0Igpgyq09PrM4YBJQQtl3t9MzkBJDbFh4NDYWwlIRkas.

Buss, Daniel F., 2009. Sustaining Life: How Human Health Depends on Biodiversity; de Eric Chivian & Aaron Bernstein. RECIIS. https://doi.org/10.3395/reciis.v3i2.262pt.

Butt, Haider, Yetisen, Ali K., Mistry, Denika, Khan, Safyan Akram, Hassan, Mohammed Umair, YunHow, Seok Hyun, 2016. *Morpho* Butterfly-Inspired Nanostructures. Adv. Opt. Mater. 4, 497–504. https://doi.org/10.1002/adom.201500658.

Capelle, Klaus., 2006. A Bird's-Eye View of Density-Functional Theory. Braz. J. Phys. https://doi.org/10.1590/s0103-97332006000700035.

Chandler, Chris J., Wilts, Bodo D., Brodie, Juliet, Vignolini, Silvia, 2017. Structural Color in Marine Algae. Adv. Opt. Mater. 5 (5), 1600646.

Chandler, Chris J., Wilts, Bodo D., Vignolini, Silvia, Brodie, Juliet, Steiner, Ullrich, Rudall, Paula J., Glover, Beverley J., Gregory, Thomas, Walker, Rachel H., 2015. Structural Colour in Chondrus Crispus. Sci. Rep. 5 (July), 11645.

Chen, Jiefu, Liu, Qing Huo, 2013. Discontinuous Galerkin Time-Domain Methods for Multiscale Electromagnetic Simulations: A Review. Proc. IEEE 101 (2), 242–254.

Chen, Xiangfan, Wang, Chen, Baker, Evan, Sun, Cheng, 2015. Numerical and Experimental Investigation of Light Trapping Effect of Nanostructured Diatom Frustules. Sci. Rep. 5 (July), 11977.

D'Alba, Liliana, Wang, Bo, Vanthournout, Bram, Shawkey, Matthew D., 2019. The Golden Age of Arthropods: Ancient Mechanisms of Colour Production in Body Scales. J. R. Soc. Interface 16 (159), 20190366.

Davis, Alexander L., Frederik Nijhout, H., Johnsen, Sönke, 2020a. Diverse Nanostructures Underlie Thin Ultra-Black Scales in Butterflies. Nat. Commun. 11 (1), 1294.

Davis, Alexander L., Thomas, Kate N., Goetz, Freya E., Robison, Bruce H., Johnsen, Sönke, Osborn, Karen J., 2020b. Ultra-Black Camouflage in Deep-Sea Fishes. Curr. Biol.: CB 30 (17), 3470–76.e3.

Dou, Shuliang, Xu, Hongbo, Zhao, Jiupeng, Zhang, Ke, Li, Na, Lin, Yipeng, Pan, Lei, Li, Yao, 2021. Bioinspired Microstructured Materials for Optical and Thermal Regulation. Adv. Mater. 33 (6), e2000697.

du Plessis, Anton, Broeckhoven, Chris, Guelpa, Anina, Roux, Stephan Gerhard le, 2017. Laboratory X-Ray Micro-Computed Tomography: A User Guideline for Biological Samples. GigaScience 6 (6), 1–11.

Dunn, A.K., Smithpeter, C.L., Welch, A.J., Richards-Kortum, R.R., 1997. Finite-Difference Time-Domain Simulation of Light Scattering from Single Cells. J. Biomed. Optics 2 (3), 262–266.

Echeverri, Sebastian A., Morehouse, Nathan I., Zurek, Daniel B., 2017. Control of Signaling Alignment during the Dynamic Courtship Display of a Jumping Spider. Behav. Ecol. 28 (6), 1445–1453.
Eliason, Chad M., Bitton, Pierre-Paul, Shawkey, Matthew D., 2013. How Hollow Melanosomes Affect Iridescent Colour Production in Birds. Proc. Biol. Sci. 280, 20131505.
Eliason, Chad M., Shawkey, Matthew D., 2012. A Photonic Heterostructure Produces Diverse Iridescent Colours in Duck Wing Patches. J. R. Soc. Interface 9 (74), 2279–2289.
Eliason, Chad M., Shawkey, Matthew D., 2014. Antireflection-Enhanced Color by a Natural Graded Refractive Index (GRIN) Structure. Optics Express 22 (Suppl 3 (May)), A642–50.
England, Grant, Kolle, Mathias, Kim, Philseok, Khan, Mughees, Muñoz, Philip, Mazur, Eric, Aizenberg, Joanna, 2014. Bioinspired Micrograting Arrays Mimicking the Reverse Color Diffraction Elements Evolved by the Butterfly Pierella Luna. Proc. Natl. Acad. Sci. U. S. A. 111 (44), 15630–15634.
Esaias, Wayne E., Curl Jr, Herbert C., 1972. Effect of Dinoflagellate Bioluminescence on Copepod Ingestion Rates. Limnol. Oceanogr. 17 (6), 901–906.
Feng, Jie, Santamouris, Mattheos, 2019. Numerical Techniques for Electromagnetic Simulation of Daytime Radiative Cooling: A Review. AIMS Mater. Sci. 6 (6), 1049–1064.
Fibics Incorporated, 2021. Introduction: Focused Ion Beam Systems. n.d. Accessed June 12. http://www.fibics.com/fib/tutorials/introduction-focused-ion-beam-systems/4/.
Francke, Mike, Kreysing, Moritz, Mack, Andreas, Engelmann, Jacob, Karl, Anett, Makarov, Felix, Guck, Jochen, et al., 2014. Grouped Retinae and Tapetal Cups in Some Teleostian Fish: Occurrence, Structure, and Function. Prog. Retin. Eye Res. 38 (January), 43–69.
Freyer, Pascal, Wilts, Bodo D., Stavenga, Doekele G., 2019. Reflections on Iridescent Neck and Breast Feathers of the Peacock, Pavo Cristatus. Interface Focus 9 (1), 20180043.
Frith, D.W., Frith, C.B., 1988. Courtship Display and Mating of the Superb Bird of Paradise Lophorina Superb. Emu - Austral Ornithol. 88 (3), 183–188.
Gallagher, Dominic F.G., Felici, Thomas P., 2003. Eigenmode Expansion Methods for Simulation of Optical Propagation in Photonics: Pros and Cons. In: Integrated Optics: Devices, Materials, and Technologies VII, 4987. International Society for Optics and Photonics, pp. 69–82.
Galusha, Jeremy W., Richey, Lauren R., Gardner, John S., Cha, Jennifer N., Bartl, Michael H., 2008. Discovery of a Diamond-Based Photonic Crystal Structure in Beetle Scales. Phys. Rev. E Stat. Nonlin. Soft Matter Phys. 77 (5 Pt 1), 050904.
Gao, Yang, Xia, Qi, Liao, Guanglan, Shi, Tielin, 2011. Sensitivity Analysis of a Bioinspired Refractive Index Based Gas Sensor. J. Bionic Eng. 8 (3), 323–334.
Gedney, Stephen D., 2011. Introduction to the Finite-Difference Time-Domain (FDTD) Method for Electromagnetics. In: Synthesis Lectures on Computational Electromagnetics, 6, pp. 1–250.
Gillis, J.M., Wibo, M., 1971. Accurate Measurement of the Thickness of Ultrathin Sections by Interference Microscopy. J. Cell Biol. 49 (3), 947–949.
Girard, Madeline B., Kasumovic, Michael M., Elias, Damian O., 2011. Multi-Modal Courtship in the Peacock Spider, Maratus Volans (O.P.-Cambridge, 1874). PLoS One 6 (9), e25390.
Goessling, Johannes W., Wardley, William P., Lopez-Garcia, Martin, 2020. Highly Reproducible, Bio-Based Slab Photonic Crystals Grown by Diatoms. Adv. Sci. 7 (10), 1903726.
Golberg, Karina, Elbaz, Amit, McNeil, Ronald, Kushmaro, Ariel, Geddes, Chris D., Marks, Robert S., 2014. Increased Bioassay Sensitivity of Bioactive Molecule Discovery Using Metal-Enhanced Bioluminescence. J. Nanoparticle Res. 16 (12), 2770.
Gonome, Hiroki, Watanabe, Kazuya, Nakamura, Kae, Kono, Takahiro, Yamada, Jun, 2020. Lighting System Bioinspired by Haworthia Obtusa. Sci. Rep. 10 (1), 11246.
Gorb, Stanislav N., 2009. Functional Surfaces in Biology: Little Structures with Big Effects Volume 1. Springer Science & Business Media.
Guidetti, G., Sun, H., Marelli, B., Omenetto, F.G., 2020. Photonic Paper: Multiscale Assembly of Reflective Cellulose Sheets in Lunaria Annua. Sci. Adv. 6 (27) https://doi.org/10.1126/sciadv.aba8966.
Haddock, Steven H.D., Dunn, Casey W., Pugh, Philip R., Schnitzler, Christine E., 2005. Bioluminescent and Red-Fluorescent Lures in a Deep-Sea Siphonophore. Science 309 (5732), 263.
Häggblad, Jon, Runborg, Olof, 2014. Accuracy of Staircase Approximations in Finite-Difference Methods for Wave Propagation. Numer. Math. 128 (4), 741–771.
Hallam, Benny T., Hiorns, Anthony G., Vukusic, Peter, 2009. Developing Optical Efficiency through Optimized Coating Structure: Biomimetic Inspiration from White Beetles. Appl. Optics 48 (17), 3243–3249.
Hansson, Tomas, Oostenbrink, Chris, Gunsteren, Wilfredf van, 2002. Molecular Dynamics Simulations. Curr. Opin. Struct. Biol. 12 (2), 190–196.
Han, Z.W., Wang, Z., Feng, X.M., Li, B., Mu, Z.Z., Zhang, J.Q., Niu, S.C., Ren, L.Q., 2016. Antireflective Surface Inspired from Biology: A Review. Biosurf. Biotribol. 2 (4), 137–150.
Haygood, M.G., Distel, D.L., 1993. Bioluminescent Symbionts of Flashlight Fishes and Deep-Sea Anglerfishes Form Unique Lineages Related to the Genus Vibrio. Nature 363 (6425), 154–156.
Henze, Miriam J., Lind, Olle, Wilts, Bodo D., Kelber, Almut, 2019. Pterin-Pigmented Nanospheres Create the Colours of the Polymorphic Damselfly Ischnura Elegans. J. R. Soc. Interface 16 (153), 20180785.
Holt, Amanda L., Sweeney, Alison M., 2016. Open Water Camouflage via 'leaky' Light Guides in the Midwater Squid Galiteuthis. J. R. Soc. Interface 13 (119), 20160230.
Holt, Amanda L., Vahidinia, Sanaz, Gagnon, Yakir Luc, Morse, Daniel E., Sweeney, Alison M., 2014. Photosymbiotic Giant Clams Are Transformers of Solar Flux. J. R. Soc. Interface 11 (101), 20140678.
Hsiung, Bor-Kai, Siddique, Radwanul Hasan, Stavenga, Doekele G., Otto, Jürgen C., Allen, Michael C., Liu, Ying, Lu, Yong-Feng, Deheyn, Dimitri D., Shawkey, Matthew D., Blackledge, Todd A., 2017. Rainbow Peacock Spiders Inspire Miniature Super-Iridescent Optics. Nat. Commun. 8 (1), 2278.
Huang, W.P., Xu, C.L., 1993. Simulation of Three-Dimensional Optical Waveguides by a Full-Vector Beam Propagation Method. IEEE J. Quantum Electron. 29 (10), 2639–2649.
Hwang, Victoria, Stephenson, Anna B., Barkley, Solomon, Brandt, Soeren, Xiao, Ming, Aizenberg, Joanna, Manoharan, Vinothan N., 2021. Designing Angle-Independent Structural Colors Using Monte Carlo Simulations of Multiple Scattering. Proc. Natl. Acad. Sci. U. S. A. 118 (4) https://doi.org/10.1073/pnas.2015551118.
Jackson, J.D., 1999. Classical Electrodynamics, 3rd Ed. Am. J. Phys. 67 (9), 841–842.
Jacobs, Matthew, Lopez-Garcia, Martin, Phrathep, O-Phart, Lawson, Tracy, Oulton, Ruth, Whitney, Heather M., 2016. Photonic Multilayer Structure of Begonia Chloroplasts Enhances Photosynthetic Efficiency. Nat. Plants 2 (11), 16162.
Jagger, W.S., 1992. The Optics of the Spherical Fish Lens. Vision Res. 32 (7), 1271–1284.
Jamin, J., 1868. Sur Un Réfracteur Différentiel Pour La Lumière Polarisée. Compte Rendus de l'Academie Des Sciences 67, 814.
Johnsen, S., 2001. Hidden in Plain Sight: The Ecology and Physiology of Organismal Transparency. Biol. Bull. 201 (3), 301–318.
Johnsen, Sönke, 2012. The Optics of Life: A Biologist's Guide to Light in Nature. Princeton University Press.
Johnson, Steven G., Joannopoulos, J.D., 2001. Block–iterative frequency–domain methods for Maxwell's equations in a planewave basis. Optics Express 8 (3), 173–190.
Jones, B.W., Nishiguchi, M.K., 2004. Counterillumination in the Hawaiian Bobtail Squid, Euprymna Scolopes Berry (Mollusca: Cephalopoda). Marine Biol. 144 (6), 1151–1155.
Karplus, M., Petsko, G.A., 1990. Molecular Dynamics Simulations in Biology. Nature 347 (6294), 631–639.
Kim, Hyeon Myeong, Lee, Gil Ju, Kim, Min Seok, Kim, Kyu Jung, Song, Young Min, 2016. Design of Bio-Inspired Morpho Butterfly Structures for Optical Sensor Applications. J. Korean Soc. Precis. Eng. 33 (5), 357–362.
Kim, Jae-Jun, Lee, Youngseop, Kim, Ha Gon, Choi, Ki-Ju, Kweon, Hee-Seok, Park, Seongchong, Jeong, Ki-Hun, 2012. Biologically Inspired LED Lens from Cuticular Nanostructures of Firefly Lantern. Proc. Natl. Acad. Sci. U. S. A. 109 (46), 18674–18678.
Kim, Jaeyoun, 2014. Absorption-Assisted Mode Transformation in Butterfly Compound Eyes. Sci. Rep. 4 (September), 6291.
Kimmel, Jyrki S., Christensen, Douglas A., 1992. Finite-Difference Time-Domain Modeling and Experimental Characterization of Planar Waveguide Fluorescence Sensors. In: Chemical, Biochemical, and Environmental Fiber Sensors III, 1587. International Society for Optics and Photonics, pp. 136–146.
Kimura, Tsubasa, Takasaki, Mihiro, Hatai, Ryosuke, Nagai, Yukiko, Uematsu, Katsuyuki, Oaki, Yuya, Osada, Minoru, et al., 2020. Guanine crystals regulated by chitin-based honeycomb frameworks for tunable structural colors of sapphirinid copepod, Sapphirina nigromaculata. Sci. Rep. 10 (1), 1–7.
Kinsler, Paul, 2011. How to Be Causal: Time, Spacetime and Spectra. Eur. J. Phys. 32 (6), 1687.
Kolle, Mathias, Lethbridge, Alfred, Kreysing, Moritz, Baumberg, Jeremy J., Aizenberg, Joanna, Vukusic, Peter, 2013. Bio-Inspired Band-Gap Tunable Elastic Optical Multilayer Fibers. Adv. Mater. https://doi.org/10.1002/adma.201203529.
Kreysing, Moritz, Pusch, Roland, Haverkate, Dorothee, Landsberger, Meik, Engelmann, Jacob, Ruiter, Janina, Mora-Ferrer, Carlos, et al., 2012. Photonic Crystal Light Collectors in Fish Retina Improve Vision in Turbid Water. Science. https://doi.org/10.1126/science.1218072.
Laman, Tim, Scholes, Edwin, 2012. Birds of Paradise: Revealing the World's Most Extraordinary Birds. National Geographic Books.
Lebedeff, A.A., 1930. L'interféromètre à Polarisation et Ses Applications. Rev. d'Opt 9, 385–413.
Lee, R. Todd, Smith, Glenn S., 2009. Detailed Electromagnetic Simulation for the Structural Color of Butterfly Wings. Appl. Optics 48 (21), 4177–4190.
Leertouwer, Hein L., Wilts, Bodo D., Stavenga, Doekele G., 2011. Refractive Index and Dispersion of Butterfly Chitin and Bird Keratin Measured by Polarizing Interference Microscopy. Optics Express 19 (24), 24061–24066.
Lee, Sanghun, Park, Sung Soo, Hagelberg, Frank, 2012. Density Functional Theory Calculation of Refractive Indices of Liquid-Forming Silicon Oil Compounds. Chem. Phys. https://doi.org/10.1016/j.chemphys.2011.12.008.
Li, Quanguo, Gao, Ke-Qin, Vinther, Jakob, Shawkey, Matthew D., Clarke, Julia A., D'Alba, Liliana, Meng, Qingjin, Briggs, Derek E.G., Prum, Richard O., 2010. Plumage Color Patterns of an Extinct Dinosaur. Science 327 (5971), 1369–1372.
Liu, Jinjie, Brio, Moysey, Moloney, Jerome V., 2012. Subpixel Smoothing Finite-Difference Time-Domain Method for Material Interface between Dielectric and Dispersive Media. Optics Lett. 37 (22), 4802–4804.
Liu, Victor, Fan, Shanhui, 2012. S4 : A Free Electromagnetic Solver for Layered Periodic Structures. Comput. Phys. Commun. 183 (10), 2233–2244.
Lotan, Oren, Bar-David, Jonathan, Smith, Cameron L.C., Yagur-Kroll, Sharon, Belkin, Shimshon, Kristensen, Anders, Levy, Uriel, 2017. Nanoscale Plasmonic V-Groove Waveguides for the Interrogation of Single Fluorescent Bacterial Cells. Nano Lett. 17 (9), 5481–5488.
Márk, Géza I., Kertész, Krisztián, Piszter, Gábor, Bálint, Zsolt, Biró, László P., 2019. First- and Second Order Light Scattering Processes in Biological Photonic Nanostructures.

NATO Science for Peace and Security Series B: Physics and Biophysics. https://doi.org/10.1007/978-94-024-1687-9_8.
Mason, C.W., 1927. Structural Colors in Insects. II. J. Phys. Chem. https://doi.org/10.1021/j150273a001.
Mata, Nathan L., Radu, Roxana A., Clemmons, Richard C., Travis, Gabriel H., 2002. Isomerization and Oxidation of Vitamin a in Cone-Dominant Retinas: A Novel Pathway for Visual-Pigment Regeneration in Daylight. Neuron 36 (1), 69–80.
McCoy, Dakota E., McCoy, Victoria E., Mandsberg, Nikolaj K., Shneidman, Anna V., Aizenberg, Joanna, Prum, Richard O., Haig, David, 2019. Structurally Assisted Super Black in Colourful Peacock Spiders. Proc. Biol. Sci. 286, 20190589.
McCoy, Dakota E., Shultz, Allison J., Vidoudez, Charles, Heide, Emma van der, Dall, Jacqueline E., Trauger, Sunia A., Haig, David, 2021. Microstructures Amplify Carotenoid Plumage Signals in Tanagers. Sci. Rep. 11 (1), 8582.
McDonald, Luke T., Narayanan, Suresh, Sandy, Alec, Saranathan, Vinodkumar, McNamara, Maria E., 2020. Brilliant Angle-Independent Structural Colours Preserved in Weevil Scales from the Swiss Pleistocene. Biol. Lett. 16 (4), 20200063.
Meiers, D.T., Heep, M.-C., von Freymann, G., 2018. Invited Article: Bragg Stacks with Tailored Disorder Create Brilliant Whiteness. APL Photonics 3 (10), 100802.
Michielsen, K., De Raedt, H., Stavenga, D.G., 2010. Reflectivity of the Gyroid Biophotonic Crystals in the Ventral Wing Scales of the Green Hairstreak Butterfly, Callophrys Rubi. J. R. Soc. Interface 7 (46), 765–771.
Milani, Marziale, Drobne, Damjana, Tatti, Francesco, 2007. How to Study Biological Samples by FIB/SEM. Mod. Res. Educ. Top. Microsc. 787–794.
Mohammadi, Ahmad, Nadgaran, Hamid, Agio, Mario, 2005. Contour-Path Effective Permittivities for the Two-Dimensional Finite-Difference Time-Domain Method. Optics Express 13 (25), 10367–10381.
Mouchet, Sébastien, Su, Bao-Lian, Tabarrant, Tijani, Lucas, Stéphane, Deparis, Olivier, 2014. Hoplia Coerulea, a Porous Natural Photonic Structure as Template of Optical Vapour Sensor. In: Photonic Crystal Materials and Devices XI, 9127:91270U. International Society for Optics and Photonics.
Moyroud, Edwige, Wenzel, Tobias, Middleton, Rox, Rudall, Paula J., Banks, Hannah, Reed, Alison, Mellers, Greg, et al., 2017. Disorder in Convergent Floral Nanostructures Enhances Signalling to Bees. Nature 550 (7677), 469–474.
Muehlberger, Michael, Ruttloff, Stephan, Nees, Dieter, Moharana, Amiya, Belegratis, Maria R., Taus, Philipp, Kopp, Sonja, Wanzenboeck, Heinz D., Prinz, Adrian, Fechtig, Daniel, 2021. Nanoimprint Replication of Biomimetic, Multilevel Undercut Nanostructures. Nanomaterials (Basel, Switzerland) 11 (4). https://doi.org/10.3390/nano11041051.
Narasimhan, Vinayak, Siddique, Radwanul Hasan, Park, Haeri, Choo, Hyuck, 2020. Bioinspired Disordered Flexible Metasurfaces for Human Tear Analysis Using Broadband Surface-Enhanced Raman Scattering. ACS Omega 5 (22), 12915–12922.
Niyogi, Krishna K., Truong, Thuy B., 2013. Evolution of Flexible Non-Photochemical Quenching Mechanisms That Regulate Light Harvesting in Oxygenic Photosynthesis. Curr. Opin. Plant Biol. 16 (3), 307–314.
Nordén, Klara K., Eliason, Chad M., Stoddard, Mary Caswell, 2021. Evolution of Brilliant Iridescent Feather Nanostructures. bioRxiv. https://doi.org/10.1101/2021.05.31.446390.
Oskooi, Ardavan F., Roundy, David, Ibanescu, Mihai, Bermel, Peter, Joannopoulos, J.D., Johnson, Steven G., 2010. Meep: A Flexible Free-Software Package for Electromagnetic Simulations by the FDTD Method. Comput. Phys. Commun. 181 (3), 687–702.
Otto, Jürgen C., Hill, David E., 2013. A New Peacock Spider from Australia Displays Three 'sapphire Gems' on a Field of Gold (Araneae: Salticidae: Euophryinae: Maratus Karsch 1878). Peckhamia 105 (1), 1–8.
Palmer, Benjamin A., Hirsch, Anna, Brumfeld, Vlad, Aflalo, Eliahu D., Pinkas, Iddo, Sagi, Amir, Rosenne, Shaked, et al., 2018. Optically Functional Isoxanthopterin Crystals in the Mirrored Eyes of Decapod Crustaceans. Proc. Natl. Acad. Sci. U. S. A. 115 (10), 2299–2304.
Palmer, Benjamin A., Taylor, Gavin J., Brumfeld, Vlad, Gur, Dvir, Shemesh, Michal, Elad, Nadav, Osherov, Aya, Oron, Dan, Weiner, Steve, Addadi, Lia, 2017. The Image-Forming Mirror in the Eye of the Scallop. Science 358 (6367), 1172–1175.
Park, Sung Soo, Lee, Sanghun, Bae, Jae Young, Hagelberg, Frank, 2011. Refractive Indices of Liquid-Forming Organic Compounds by Density Functional Theory. Chem. Phys. Lett. 511 (4), 466–470.
Pedrotti, Frank L., Pedrotti, Leno M., Pedrotti, Leno S., 2017. Introduction to Optics. Cambridge University Press.
Plass, Gilbert N., Kattawar, George W., 1967. Monte Carlo Calculations of Light Scattering From Clouds. https://doi.org/10.21236/ad0657363.
Poladian, Leon, Wickham, Shelley, Lee, Kwan, Large, Maryanne C.J., 2009. Iridescence from Photonic Crystals and Its Suppression in Butterfly Scales. J. R. Soc. Interface. https://doi.org/10.1098/rsif.2008.0353.focus.
Potter, Mike, Bérenger, Jean-Pierre, 2017. A Review of the Total Field/scattered Field Technique for the FDTD Method. FERMAT 19, 1–13.
Potyrailo, Radislav A., Bonam, Ravi K., Hartley, John G., Starkey, Timothy A., Vukusic, Peter, Vasudev, Milana, Bunning, Timothy, et al., 2015. Towards Outperforming Conventional Sensor Arrays with Fabricated Individual Photonic Vapour Sensors Inspired by Morpho Butterflies. Nat. Commun. 6 (September), 7959.
Pris, Andrew D., Utturkar, Yogen, Surman, Cheryl, Morris, William G., Vert, Alexey, Zalyubovskiy, Sergiy, Deng, Tao, Ghiradella, Helen T., Potyrailo, Radislav A., 2012. Towards High-Speed Imaging of Infrared Photons with Bio-Inspired Nanoarchitectures. Nat. Photonics 6 (3), 195–200.
Rao, Sathyanarayan, 2016. "Two Dimensional Wave Interference Using Finite Difference Time Domain Method (FDTD)." MATLAB Central File Exchange. 2016. https://www.mathworks.com/matlabcentral/fileexchange/55301-two-dimensional-wave-interference-using-finite-difference-time-domain-method-fdtd.
Rassart, Marie, Simonis, Priscilla, Bay, Annick, Deparis, Olivier, Vigneron, Jean Pol, 2009. Scale Coloration Change Following Water Absorption in the Beetle Hoplia Coerulea (Coleoptera). Phys. Rev. E Stat. Nonlin. Soft Matter Phys. 80 (3 Pt 1), 031910.
Regan, Emma C., Shen, Yichen, Lopez, Josue J., Hsu, Chia Wei, Zhen, Bo, Joannopoulos, John D., Soljačić, Marin, 2016. Substrate-Independent Light Confinement in Bioinspired All-Dielectric Surface Resonators. ACS Photonics 3 (4), 532–536.
Rosenthal, Eric I., Holt, Amanda L., Sweeney, Alison M., 2017. Three-Dimensional Midwater Camouflage from a Novel Two-Component Photonic Structure in Hatchetfish Skin. J. R. Soc. Interface 14 (130). https://doi.org/10.1098/rsif.2016.1034.
Rylander, Thomas, Ingelström, Par, Bondeson, Anders, 2013. Computational Electromagnetics. Springer, New York, NY.
Saba, Matthias, Wilts, Bodo D., Hielscher, Johannes, Schröder-Turk, Gerd E., 2014. Absence of Circular Polarisation in Reflections of Butterfly Wing Scales with Chiral Gyroid Structure. Mater. Today: Proc. 1 (January), 193–208.
Saijonmaa, J., Yevick, D., 1983. Beam-Propagation Analysis of Loss in Bent Optical Waveguides and Fibers. JOSA 73 (12), 1785–1791.
Sandt, Joseph D., Moudio, Marie, Kenji Clark, J., Hardin, James, Argenti, Christian, Carty, Matthew, Lewis, Jennifer A., Kolle, Mathias, 2018. Stretchable Optomechanical Fiber Sensors for Pressure Determination in Compressive Medical Textiles. Adv. Healthcare Mater. 7 (15), e1800293.
Sankaran, Krishnaswamy, 2019. Are You Using the Right Tools in Computational Electromagnetics? Eng. Rep. 1 (3) https://doi.org/10.1002/eng2.12041.
Saranathan, Vinodkumar, Forster, Jason D., Noh, Heeso, Liew, Seng-Fatt, Mochrie, Simon G.J., Cao, Hui, Dufresne, Eric R., Prum, Richard O., 2012. Structure and Optical Function of Amorphous Photonic Nanostructures from Avian Feather Barbs: A Comparative Small Angle X-Ray Scattering (SAXS) Analysis of 230 Bird Species. J. R. Soc. Interface 9 (75), 2563–2580.
Sasov, A., Pauwels, B., Bruyndonckx, P., Liu, X., McNulty, Ian, Eyberger, Catherine, Lai, Barry, 2011. New Lens-Free X-Ray Source for Laboratory Nano-CT with 50-Nm Spatial Resolution. https://doi.org/10.1063/1.3625324.
Schertel, Lukas, van de Kerkhof, Gea T., Jacucci, Gianni, Catón, Laura, Ogawa, Yu, Wilts, Bodo D., Ingham, Colin J., Vignolini, Silvia, Johansen, Villads E., 2020. Complex Photonic Response Reveals Three-Dimensional Self-Organization of Structural Coloured Bacterial Colonies. J. R. Soc. Interface 17 (166), 20200196.
Seo, Han-Bok, Lee, Seung-Yop, 2017. Bio-Inspired Colorimetric Film Based on Hygroscopic Coloration of Longhorn Beetles (Tmesisternus Isabellae). Sci. Rep. 7 (March), 44927.
Sheng, Xin-Qing, Song, Wei, 2011. Essentials of Computational Electromagnetics. John Wiley & Sons.
Siddique, Radwanul Hasan, Diewald, Silvia, Leuthold, Juerg, Hölscher, Hendrik, 2013. Theoretical and Experimental Analysis of the Structural Pattern Responsible for the Iridescence of Morpho Butterflies. Optics Express 21 (12), 14351–14361.
Siddique, Radwanul Hasan, Donie, Yidenekachew J., Gomard, Guillaume, Yalamanchili, Sisir, Merdzhanova, Tsvetelina, Lemmer, Uli, Hölscher, Hendrik, 2017. Bioinspired Phase-Separated Disordered Nanostructures for Thin Photovoltaic Absorbers. Sci. Adv. 3 (10), e1700232.
Skou, Soren, Gillilan, Richard E., Ando, Nozomi, 2014. Synchrotron-Based Small-Angle X-Ray Scattering of Proteins in Solution. Nat. Protocols 9 (7), 1727–1739.
Smentkowski, V., Ostrowski, S., Olson, E., Cournoyer, J., Dovidenko, K., Potyrailo, R., 2006. Exploration of a Butterfly Wing Using a Diverse Suite of Characterization Techniques. Microsc. Microanal. 12 (S02), 1228–1229.
Spinner, Marlene, Kovalev, Alexander, Gorb, Stanislav N., Westhoff, Guido, 2013. Snake Velvet Black: Hierarchical Micro- and Nanostructure Enhances Dark Colouration in Bitis Rhinoceros. Sci. Rep. 3, 1846.
Stavenga, Doekele G., van Barneveld, H.H., 1975. On Dispersion in Visual Photoreceptors. Vision Res. 15 (October), 1091–1095.
Stavenga, Doekele G., Kooi, Casper J. van der, Wilts, Bodo D., 2017. Structural Coloured Feathers of Mallards Act by Simple Multilayer Photonics. J. R. Soc. Interface 14 (133). https://doi.org/10.1098/rsif.2017.0407.
Stavenga, Doekele G., Leertouwer, Hein L., Hariyama, Takahiko, De Raedt, Hans A., Wilts, Bodo D., 2012. Sexual Dichromatism of the Damselfly Calopteryx japonica Caused by a Melanin-Chitin Multilayer in the Male Wing Veins. PLoS One. https://doi.org/10.1371/journal.pone.0049743.
Stavenga, Doekele G., Leertouwer, Hein L., Osorio, Daniel C., Wilts, Bodo D., 2015. High Refractive Index of Melanin in Shiny Occipital Feathers of a Bird of Paradise. Light Sci. Appl. 4 (1) e243–e243.
Stavenga, Doekele G., Leertouwer, Hein L., Wilts, Bodo D., 2013. Quantifying the Refractive Index Dispersion of a Pigmented Biological Tissue Using Jamin–Lebedeff Interference Microscopy. Light Sci. Appl. 2 (9) e100–e100.
Stavenga, Doekele G., Leertouwer, Hein L., Wilts, Bodo D., 2018. Magnificent Magpie Colours by Feathers with Layers of Hollow Melanosomes. J. Exp. Biol. 221 (Pt 4) https://doi.org/10.1242/jeb.174656.
Stavenga, Doekele G., Otto, Jürgen C., Wilts, Bodo D., 2016. Splendid Coloration of the Peacock Spider Maratus Splendens. J. R. Soc. Interface 13 (121). https://doi.org/10.1098/rsif.2016.0437.
Stavenga, Doekele G., Wilts, Bodo D., 2019. Measuring the Refractive Index Dispersion of (un)pigmented Biological Tissues by Jamin-Lebedeff Interference Microscopy. AIP Adv. https://doi.org/10.1063/1.5113485.
Steindorfer, Michael A., Schmidt, Volker, Belegratis, Maria, Stadlober, Barbara, Krenn, Joachim R., 2012. Detailed simulation of structural color generation inspired by the *Morpho* butterfly. Optics Express 20, 21485–21494.
Stevens, Martin, Merilaita, Sami, 2011. Animal Camouflage: Mechanisms and Function. Cambridge University Press.

Stratakis, E., Bonse, J., Heitz, J., Siegel, J., Tsibidis, G.D., Skoulas, E., Papadopoulos, A., et al., 2020. Laser Engineering of Biomimetic Surfaces. Mater. Sci. Eng. R Rep.: Rev. J. 141 (July), 100562.
Sullivan, Dennis M., 2013. Electromagnetic Simulation Using the FDTD Method. John Wiley & Sons.
Taflove, Allen, 2007. A Perspective on the 40-Year History of FDTD Computational Electrodynamics. Appl. Comput. Electromagn. Soc. J. 22 (1), 1–21.
Taflove, Allen, Hagness, Susan C., Piket-May, Melinda, 2005. Computational electromagnetics: the finite-difference time-domain method. The Electrical Engineering Handbook, 3rd ed. Elsevier Academic Press.
Tanifuji, T., Ohtomo, T., Ishikawa, T., Ichitsubo, K., 2004. Time-Resolved Reflectance of an Optical Pulse from an Adult Head Model Utilizing the Finite Difference Time Domain (FDTD) Analysis. Conference Proceedings: … Annual International Conference of the IEEE Engineering in Medicine and Biology Society. IEEE Engineering in Medicine and Biology Society. Conference 2004 1248–1251.
Tornberg, Anna-Karin, Engquist, Björn, 2008. Consistent Boundary Conditions for the Yee Scheme. J. Comput. Phys. https://doi.org/10.1016/j.jcp.2008.03.045.
Vacquié-Garcia, Jade, Royer, François, Dragon, Anne-Cécile, Viviant, Morgane, Bailleul, Frédéric, Guinet, Christophe, 2012. Foraging in the Darkness of the Southern Ocean: Influence of Bioluminescence on a Deep Diving Predator. PLoS One 7 (8), e43565.
Verstraete, Charlotte, Mouchet, Sébastien R., Verbiest, Thierry, Kolaric, Branko, 2019. Linear and Nonlinear Optical Effects in Biophotonic Structures Using Classical and Nonclassical Light. J. Biophotonics 12 (1), e201800262.
Vigneron, Jean Pol, Simonis, Priscilla, Aiello, Annette, Bay, Annick, Windsor, Donald M., Colomer, Jean-François, Rassart, Marie, 2010. Reverse Color Sequence in the Diffraction of White Light by the Wing of the Male Butterfly Pierella Luna (Nymphalidae: Satyrinae). Phys. Rev. E Stat. Nonlin. Soft Matter Phys. 82 (2 Pt 1), 021903.
Vignolini, Silvia, Rudall, Paula J., Rowland, Alice V., Reed, Alison, Moyroud, Edwige, Faden, Robert B., Baumberg, Jeremy J., Glover, Beverley J., Steiner, Ullrich, 2012. Pointillist Structural Color in Pollia Fruit. Proc. Natl. Acad. Sci. U. S. A. 109 (39), 15712–15715.
Vukusic, Peter, Sambles, J. Roy, 2003. Photonic Structures in Biology. Nature 424 (6950), 852–855.
Vukusic, Peter, Sambles, J. Roy, Lawrence, C.R., 2004. Structurally assisted blackness in butterfly scales. Proc. R. Soc. B Biol. Sci. 271, 237–239. https://doi.org/10.1098/rsbl.2003.0150.
Vukusic, Peter, Stavenga, D.G., 2009. Physical Methods for Investigating Structural Colours in Biological Systems. J. R. Soc. Interface 6 (Suppl 2 (April)), S133–48.
Wang, Wanlin, Zhang, Wang, Zhang, Di, Wang, Guo Ping, 2017. A Low-Cost, High-Efficiency Light Absorption Structure Inspired by the Papilio Ulysses Butterfly. RSC Adv. 7 (37), 22749–22756.
Wang, Yongguo, Ren, Yuehong, Wang, Zhijun, Xu, Qin, Zhang, Lei, 2020. Study on the Microstructure and Its Coloration Mechanism of Peacock Feather by the FDTD Method. J. Phys. Conf. Ser. 1549 (3), 032036.
Wang, Zhong Lin, Lee, Jean L., 2008. 9 - Electron Microscopy Techniques for Imaging and Analysis of Nanoparticles. In: Kohli, Rajiv, Mittal, K.L. (Eds.), Developments in Surface Contamination and Cleaning. William Andrew Publishing, Norwich, NY, pp. 531–584.
Wan, Nan, Weng, Lingdong, Zhu, Hao, Du, Jihe, Lin, Xiaogang, 2017. FDTD Method and Models in Optical Education. 14th Conference on Education and Training in Optics and Photonics: ETOP 2017. https://doi.org/10.1117/12.2268324.
Weaver, Ryan J., Santos, Eduardo S.A., Tucker, Anna M., Wilson, Alan E., Hill, Geoffrey E., 2018. Carotenoid Metabolism Strengthens the Link between Feather Coloration and Individual Quality. Nat. Commun. 9 (1), 73.
Widder, Edith A., 1998. A Predatory Use of Counterillumination by the Squaloid Shark, Isistius Brasiliensis. Environ. Biol. Fishes 53 (3), 267–273.
Wildman, Jack, Denis, Jean-Christophe, Repiščák, Peter, Paterson, Martin J., Galbraith, Ian, 2016. Molecular Dynamics Simulations for the Study of Optical Properties in Conjugated Semiconducting Molecules. In, 2016:P33.001.
Wilts, Bodo D., Matsushita, Atsuko, Arikawa, Kentaro, Stavenga, Doekele G., 2015. Spectrally Tuned Structural and Pigmentary Coloration of Birdwing Butterfly Wing Scales. J. R. Soc. Interface 12 (111), 20150717.
Wilts, Bodo D., Michielsen, Kristel, Raedt, Hans De, Stavenga, Doekele G., 2014. Sparkling Feather Reflections of a Bird-of-Paradise Explained by Finite-Difference Time-Domain Modeling. Proc. Natl. Acad. Sci. U. S. A. 111 (12), 4363–4368.
Wilts, Bodo D., Michielsen, Kristel, Kuipers, Jeroen, Raedt, Hans De, Stavenga, Doekele G., 2012. Brilliant Camouflage: Photonic Crystals in the Diamond Weevil, Entimus Imperialis. Proc. Biol. Sci. 279 (1738), 2524–2530.
Wilts, Bodo D., Otto, Jürgen, Stavenga, Doekele G., 2020. Ultra-Dense, Curved, Grating Optics Determines Peacock Spider Coloration. Nanoscale Adv. 2 (3), 1122–1127.
Wilts, Bodo D., Pirih, Primož, Arikawa, Kentaro, Stavenga, Doekele G., 2013. Shiny Wing Scales Cause Spec(tac)ular Camouflage of the Angled Sunbeam Butterfly, Curetis Acuta. Biol. J. Linn. Soc. 109 (2), 279–289.
Wilts, Bodo D., Rudall, Paula J., Moyroud, Edwige, Gregory, Tom, Ogawa, Yu, Vignolini, Silvia, Steiner, Ullrich, Glover, Beverley J., 2018a. Ultrastructure and Optics of the Prism-like Petal Epidermal Cells of Eschscholzia Californica (California Poppy). New Phytol. 219 (3), 1124–1133.
Wilts, Bodo D., Sheng, Xiaoyuan, Holler, Mirko, Diaz, Ana, Guizar-Sicairos, Manuel, Raabe, Jörg, Hoppe, Robert, et al., 2018b. Evolutionary-Optimized Photonic Network Structure in White Beetle Wing Scales. Adv. Mater. https://doi.org/10.1002/adma.201702057.
Wilts, Bodo D., Wijnen, Bas, Leertouwer, Hein L., Steiner, Ullrich, Stavenga, Doekele G., 2017. Extreme Refractive Index Wing Scale Beads Containing Dense Pterin Pigments Cause the Bright Colors of Pierid Butterflies. Adv. Opt. Mater. 5 (3), 1600879.
Xie, Guoyong, Zhang, Guoming, Lin, Feng, Zhang, Jin, Liu, Zhongfan, Mu, Shichen, 2008. The Fabrication of Subwavelength Anti-Reflective Nanostructures Using a Bio-Template. Nanotechnology. https://doi.org/10.1088/0957-4484/19/9/095605.
Yamashita, Kazuma, Fukihara, Midori, Hirai, Yoshihiko, Kuwahara, Yuji, Saito, Akira, 2020. Elucidating the Mystery of Morpho-Blue Using in-Plane Randomness: Toward Simple Nanofabrication. Jpn. J. Appl. Phys. 59 (5), 052009.
Yasir, Mohammad, Sai, Tianqi, Sicher, Alba, Scheffold, Frank, Steiner, Ullrich, Wilts, Bodo D., Dufresne, Eric R., 2021. Enhancing the Refractive Index of Polymers with a Plant-Based Pigment. arXiv cond-Mat.soft. arXiv. http://arxiv.org/abs/2105.07434.
Yee, Kane, 1966. Numerical Solution of Initial Boundary Value Problems Involving Maxwell's Equations in Isotropic Media. IEEE Trans. Antennas Propag. 14 (3), 302–307.
Yoneda, Satoshi, Ito, Fuyu, Yamanaka, Shigeru, Usami, Hisanao, 2016. Optical Properties of Nanoporous Silica Frustules of a Diatom Determined Using a 10 μm Microfiber Probe. Jpn. J. Appl. Phys. 55 (7), 072001.
Young, Richard Edward, Kampa, Elizabeth M., Maynard, Sherwood D., Mencher, Frederick M., Roper, Clyde F.E., 1980. Counterillumination and the Upper Depth Limits of Midwater Animals. Deep Sea Res. Part A Oceanogr. Res. Pap. 27 (9), 671–691.
Yun, Geun-Tae, Jung, Woo-Bin, Oh, Myung Seok, Jang, Gyu Min, Baek, Jieung, Kim, Nam Il, Im, Sung Gap, Jung, Hee-Tae, 2018. Springtail-Inspired Superomniphobic Surface with Extreme Pressure Resistance. Sci. Adv. 4 (8), eaat4978.
Yu, Wenhua, Mittra, R., 2001. A Conformal Finite Difference Time Domain Technique for Modeling Curved Dielectric Surfaces. IEEE Microwave Wireless Compon. Lett. 11 (1), 25–27.
Zhang, Haiwen, Ly, Kally C.S., Liu, Xianghui, Chen, Zhihan, Yan, Max, Wu, Zilong, Wang, Xin, Zheng, Yuebing, Zhou, Han, Tongxiang, Fan, 2020. Biologically Inspired Flexible Photonic Films for Efficient Passive Radiative Cooling. Proc. Natl. Acad. Sci. U. S. A. 117 (26), 14657–14666.
Zhao, Qibin, Fan, Tongxiang, Ding, Jian, Zhang, Di, Guo, Qixin, Kamada, Masao, 2011. Super Black and Ultrathin Amorphous Carbon Film Inspired by Anti-Reflection Architecture in Butterfly Wing. Carbon 49 (3), 877–883.
Zhou, Lei, Ou, Qing-Dong, Chen, Jing-De, Shen, Su, Tang, Jian-Xin, Li, Yan-Qing, Shuit-Tong, Lee, 2014. Light Manipulation for Organic Optoelectronics Using Bio-Inspired Moth's Eye Nanostructures. Sci. Rep. 4 (February), 4040.
Zhu, Caigang, Liu, Quan, 2013. Review of Monte Carlo Modeling of Light Transport in Tissues. J. Biomed. Optics 18 (5), 50902.